THE
PHYSICAL REVIEW
A Journal of Experimental and Theoretical Physics
VOL. 45, No. 5 MARCH 1, 1934 SECOND SERIES

# On the Isotopic Ratio in Oxygen

W. R. SMYTHE, *California Institute of Technology*
(Received December 30, 1933)

A new mass-spectrometer has been constructed along lines previously described in which the defects that appeared in the first apparatus are eliminated. The electrostatic analyzer has been slightly altered to take full advantage of its focussing properties for which a formula is given. Because of the faintness of the scattered background, very weak peaks can be measured precisely. Oxygen, prepared by the decomposition of $PbO_2$, has been analyzed and the ratio of the amount of $O^{16}$ to $O^{18}$ found to be 503 $\pm 10$. It is suggested that the discrepancy between this and previous values may be due to the method of preparation of the oxygen sample.

THE theory of one method of using alternating electric fields to select, from a beam of charged particles, all those having a certain velocity, has been worked out in a previous paper.[1] In this paper it was pointed out that to be passed by the filter the given particle must satisfy two conditions. First, its displacement on leaving the field must be less than the width of the last slit, and, second, its angular deviation must be small enough to enable it to pass through subsequent slits. Two filters, depending chiefly on the first criterion for selectivity have been constructed and described.[2,3] Neither of these pieces of apparatus came up to expectations as to resolving power and background and in one case bad "ghosts" rendered the apparatus almost useless. Both used more symmetrical fields than the theory requires and both separated the two halves of the field by a considerable distance, thus, theoretically, greatly increasing the resolving power but involving construction complications. The apparatus described in this paper uses unsymmetrical fields and long collimating sections, thus bringing in the second criterion for selection as well as the first. The two halves of the fields are adjacent, the electrical connections on the second half being reversed to produce the required 180° phase difference. No relative displacement for different velocity ranges is necessary and a more rigid and precise mechanical construction is possible. The theoretical resolving power is about one-seventh that of the original apparatus but is completely attained experimentally.

The theory applicable to the second condition for selection may be obtained quite simply from that originally published.[1] Using Eq. (2) and Eq. (6) of this paper we find that at a distance $d$ beyond the end of the first field the additional displacement of the particle due to its emergent lateral velocity is

$$y' = 2Wn^2\pi^2 d(\Delta v/v_0)^2/a,$$

where $W$ is the total spread of the beam at the center of the fields, $2n$ is the number of oscillations of the electric field during its passage, $4a$ is the total length of the field and $\Delta v$ is the

[1] W. R. Smythe, Phys. Rev. **28**, 1275 (1926).
[2] Smythe and Mattauch, Phys. Rev. **40**, 429 (1932).
[3] Mattauch, Phys. Zeits. **33**, 899 (1932).

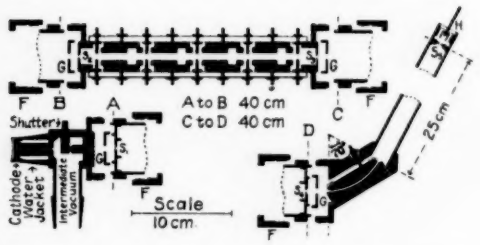


FIG. 1. Section of the new mass-spectrometer showing cathode with canals, collimating slits, $S_1$ and $S_2$ for the entering beam and $S_3$ and $S_4$ for the emerging beam, condenser section, electrostatic deflecting field and receiving slit, $S_5$, with Faraday cylinder, $H$.

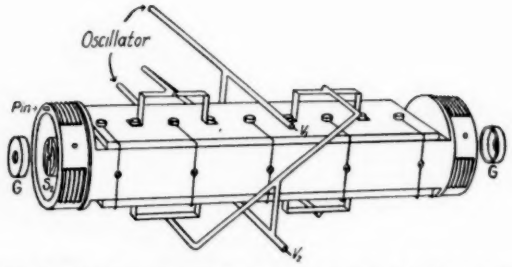


FIG. 2. Condenser section of apparatus showing mounting of slits, electrical connections and "breech block" method of joining sections.

difference between its velocity and $v_0$, the undeviated velocity. The derivation of the formula indicates that this selection condition is most effective on those phases in which the first is least effective and *vice versa*. It is specially efficient in eliminating large values of $\Delta v$ since this quantity occurs squared. This is borne out experimentally as the scattered background a short distance away from the peaks in the present apparatus is fifty times smaller than in the first.

The actual construction of the condenser section of the filter is shown in section at the top of Fig. 1. The four upper condenser plates and the five upper diaphragm halves are mounted on a strip of plate glass and carefully adjusted as to spacing and alignment with indicating gauges. The lower system is then similarly assembled and the whole mounted on the brass frame, the two faces of which are accurately parallel. Plate glass strips on the sides of the plates insure permanent alignment. All joints are closed outside with a small fillet of beeswax, which has been boiled under reduced pressure, and then painted with glyptal lacquer. These joints have been permanently tight and give off no detectable amount of vapor. An external view of the condenser mounting, with the electrical connections in place, is shown in Fig. 2. There are four slits to be lined up: $S_1$, $S_2$, $S_3$ and $S_4$ in Fig. 1. First $S_2$ and $S_3$ are set on the axis of the condenser system, then the collimating tubes are attached and $S_1$ and $S_4$ are lined up with them. The latter operation is greatly facilitated by the mounting of the slit jaws, shown in Fig. 2, which permits one to see around them during adjustment. When this is finished the perforated cap, $G$, is placed over the slit permitting the positive rays to pass between the jaws only.

To insure accurately reproducible assembling of the apparatus gaskets were dispensed with. The sections to be joined were fitted together as shown in Fig. 1 and Fig. 2, a pin, not shown, preventing relative rotation. The collars, marked $F$ in Fig. 1, with sectored threads, are then slid over and the joints secured tightly by an eighth turn of the collars. Each end of a collar is rendered vacuum tight by a fillet of beeswax run around it with a hot wire. After such a joint has once been sealed it can be opened in ten seconds and closed, vacuum tight, in five minutes and the alignment is perfect. The water-cooled cathode, the channels separating the discharge tube from the intermediate vacuum and the latter from the high vacuum and a shutter for excluding the positives are shown at the lower left corner of Fig. 1.

The electrostatic analyzing field, shown at the lower right of Fig. 1 has been changed somewhat from that used in previous apparatus[2] to secure better resolution and focussing with approximately the same dimensions as before. Although we were aware that a certain amount of focussing of the beam was present in our original electrostatic analyzer where the receiving slit is some distance beyond the edge of the electric field, it did not occur to us that it might come at the same point as the best angular resolving power until a perusal of the paper by Hughes and Rojansky[4] suggested the possibility. For the voltages, slit widths and resolving power that we need, their arrangement is somewhat cumbersome but a similar analysis may be applied to our case.

[4] Hughes and Rojansky, Phys. Rev. **34**, 284 (1929).

To compute the arrangement for maximum resolving power we assume that all particles have the same charge and enter the radial cylindrical electric field normal to the lines of force at the point $\theta=0$, $r=r_0$, moving with a velocity $v$. If the particle of mass $m_0$ travels in a circular path of radius $r_0$, then the central force acting on a particle of mass $m$ will be $F=ma=-m_0v^2/r$, and its equations of motion will be

$$\ddot{r}-r\dot{\theta}^2=-m_0v^2/(mr) \tag{1}$$

and

$$d(r^2\dot{\theta})/dt=0. \tag{2}$$

Integrating (2) gives $r^2\dot{\theta}=r_0^2\dot{\theta}_0=r_0v$, or $\dot{\theta}=vr_0/r^2$. Substituting for $d/dt$ its equivalent $\dot{\theta}d/d\theta$ in Eq. (1) and letting $r=r_0m^{1/2}/(um_0^{1/2})$ we obtain the form

$$d^2u/d\theta^2=(1/u)-u.$$

It may be verified that the expression

$$u=1+\epsilon\cos(2^{1/2}\theta)+\epsilon^2(1/4-1/6\cos(2^{1/2}\theta)-1/12\cos(2\cdot 2^{1/2}\theta))$$

satisfies this equation if we neglect the cube and higher powers of $\epsilon$. This expression, which we owe to Dr. Huff, may be simplified in our case. When $\theta=0$, $r=r_0$ so that $\epsilon=(m/m_0)^{1/2}-1$, which, as we are only interested in values of $m$ close to $m_0$, is a very small quantity. We shall include only the first power terms in $\epsilon$. Substituting for $u$ and $\epsilon$, multiplying through by $(m_0/m)^{1/2}$ and subtracting both sides from one gives

$$(r-r_0)/r=[1-(m_0/m)^{1/2}][1-\cos(2^{1/2}\theta)].$$

Let $x_1$ be the amount, $r-r_0$, which the mass $m$ is displaced from the mass $m_0$ at $\theta_1$, where they emerge from the field. Substitute $\Delta$ for $1-(m_0/m)^{1/2}$ giving

$$x_1=r\Delta[1-\cos(2^{1/2}\theta_1)].$$

If $\phi$ is the angle between the paths of $m_0$ and $m$ on emerging from the field, then

$$\tan\phi=dx_1/rd\theta=2^{1/2}\Delta\sin(2^{1/2}\theta_1).$$

The total amount that $m$ will be displaced from $m_0$ at a distance $R$ beyond the edge of the field will be $x=x_1+R\tan\phi$. For best resolving power $dx/d\theta=0$. Thus

$$\tan(2^{1/2}\theta_1)=-2^{1/2}R/r_0 \tag{3}$$

since $r=r_0$ approximately.

It is not difficult to show, by a method similar to that used by Hughes and Rojansky, that this is also the condition that a homogeneous beam, slightly divergent on entering the field, be brought to a focus at $S_5$ (Fig. 1), a distance $R$ beyond the edge of the field, after being bent through an angle $\theta_1$, 70° in Fig. 1. If $R=0$ this reduces to their special case.

The oscillator used with this apparatus is the same already described.[2] As Dr. Mattauch pointed out in a letter to the author, one cannot be certain, no matter how symmetrical the system seems to be, that the voltage halfway between the plates will always be zero. Therefore we have now grounded the center of the oscillator coil through a R.F. choke and use a compensator connected across the leads by which earth capacitance can be shifted from one side of the line to the other until $V_1=-V_2$ (Fig. 2). This adjustment is different for 30, 40 and 60 meter wave-lengths. The r.m.s. voltage between $V_1$ and $V_2$ is now indicated by a permanently connected, specially constructed, electrostatic voltmeter which can be read to 0.1 percent. Each side of this has an identical capacitance to ground.

Only minor changes have been made in the discharge tube from that previously described.[2] The electrometer system and the scheme of using the electrostatic field as a shutter for positive rays is also the same as before. The pumping system now consists of a two stage glass butyl phthalate diffusion pump backed by a hyvac. One stage pumps from the high vacuum part of the apparatus, which includes the collimating sections, the condenser section, the deflecting field section and the Faraday cylinder. This stage delivers to the other stage which pumps from the region between the channels. Diffusion and creepage of the pump liquid into the apparatus is prevented by charcoal lined tubes. This pumping system is very satisfactory and liquid air is unnecessary.

Naturally, since the whole adjustment was done with oxygen, the first measurements undertaken were on this element. There are now no "ghosts" and the scattered background is very small (see Fig. 3) so that precise measurements of weak peaks are possible. Systematic errors in comparing weak currents with strong currents

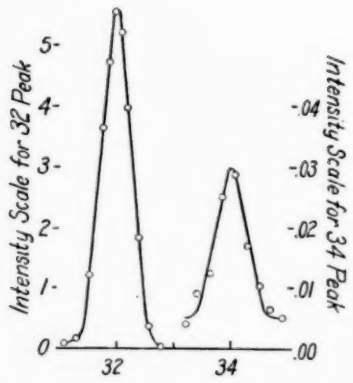


FIG. 3. Oxygen molecule peaks run with low resolving power. Oscillating r.m.s. voltage, $V^{32}=160$ volts, $V^{34}=170$ volts. Wave-length 60 meters.

have been eliminated as already described.[2] The peaks chosen were $32(O^{16}O^{16})$ and $34(O^{18}O^{16})$. To make certain that both molecules travel identical paths in the apparatus the oscillating voltage $V^{32}$ used in measuring the 32 peak and the voltage $V^{34}$ used on the 34 peak were always kept in the ratio $V^{32}/V^{34}=32/34$. The only correction therefore to be applied to the measured peaks is that due to the voltage distribution in the discharge tube. This was determined for each run by shutting off the oscillator and measuring the total positive ion current at the deflecting voltage used for 32 and at that used for 34. This intensity ratio turned out to be surprisingly constant and deviated less than one percent from 1.167 for a variation of 80 percent in the discharge tube current. The actual ratio of the number of $O^{16}O^{16}$ to $O^{18}O^{16}$ molecules is therefore given by $1.167I^{32}/I^{34}$ where $I^{32}$ and $I^{34}$ are the measured intensities of the two peaks.

A typical pair of peaks, obtained with low resolving power in a preliminary run, is shown in Fig. 3. No complete peaks were run with the higher precision used in the final measurements. The curve drawn for the 34 peak is identical in shape with the 32 peak. When the resolving power is increased by raising the oscillator voltage the 33 peak appears. In some cases there is a peak at 31 whose intensity varies independently from that of the oxygen peaks and which is perhaps due to $Na_2O^{++}$, since the sodium $D$ lines frequently appear in the discharge tube. It seems that the increase of the speed of measurement due to the larger intensity at low resolving power is offset by the overlapping of the base of the 33 and 34 peaks. It was finally decided to use higher resolving power and, after locating the top of the 32 peak accurately, measure only four points, the top of the 32 peak and the top and background at each side of the 34 peak. This enables more runs to be made and gives ample time to make the two weak background measurements with precision before the discharge conditions can change.

The oxygen was prepared by the thermal decomposition of $PbO_2$ at the pressure in the discharge tube, about 0.05 mm Hg. Impurities, chiefly water vapor, were frozen out in a liquid air trap so that the spectrum of the discharge tube showed only oxygen lines and bands and sodium lines. The latter appeared to come from a yellow glow on the surface of the glass. Between atomic weights 10 and 40 no other peaks were found with an intensity as great as five percent of that of the oxygen. In adjusting the apparatus a large charge of $PbO_2$ was used and the temperature required to maintain the oxygen pressure was constant within a degree or two for weeks. Finally it became necessary to raise the temperature rather rapidly to maintain the pressure and at this point the relative amount of $O^{18}O^{16}$ increased sharply for a short time and then relapsed to its former value. Since no record had been kept of temperature or time of heating, during preliminary adjustments, it was decided to repeat with a smaller amount of $PbO_2$ to save time. This was a mistake because the effect will be washed out if this phase passes so rapidly that the new composition cannot be established throughout the volume of the apparatus. Furthermore, we were unfortunate in getting no readings at this critical point as we did not recognize it until plotting the data next day. It apparently falls between 4 and 5 in Table I

TABLE I. *Abundance ratio* $O^{16}/O^{18}$.

| No. | Temp. (°C) | Time (hours) | MA Tube current | Ratio $O^{16}/O^{18}$ |
|---|---|---|---|---|
| 1 | 290° | 28 | 10.0 | 502 |
| 2 | 292° | 34 | 7.5 | 499 |
| 3 | 295° | 42 | 7.7 | 510 |
| 4 | 300° | 49 | 7.0 | 491 |
| 5 | 310° | 57 | 8.7 | (524) |
| 6 | 318° | 63 | 6.0 | 512 |
| 7 | 323° | 68 | 7.3 | (492) |

because the readings in 4 were falling slowly and those in 5 were rising rapidly. For determining the average composition of the oxygen, however, the data are adequate. The apparatus was turned on in the morning and off at night. Each afternoon two or three determinations of the ratio were made. The mean of each set is included in the table and none are omitted. In two cases, 5 and 7, an individual reading deviates more than 10 from the mean of that day and so these sets were discarded in averaging although the result is little changed by including them. The current in the discharge tube is also given. Larger current indicates higher pressure. The r.m.s. oscillating voltages are: $V^{32}=200$ volts, $V^{34}=212.5$ volts.

The mean of these values, excluding 5 and 7, is 503. The maximum deviations are $+9$ and $-12$ so that it is probably safe to say that this value is correct to $\pm 10$ for our sample of oxygen. It should be noted that this value is considerably lower than any previously given. Aston[5] gives 535, Mecke and Childs (spectroscopic)[6] give 640 and Kallman and Lasareff[7] give 630. Workers at the University of California have found that a partial separation of the oxygen as well as of the hydrogen takes place in electrolysis so that electrolytic oxygen should give too high a value. Most of the oxygen on the earth has been used in oxidizing the earth's crust and only a small fraction of one percent remains in the air. It is possible that some concentration, probably of the $O^{16}$, has taken place in this process so that the ratio for air is above average. In our sample the method of preparation of the $PbO_2$ is unknown. It was made by Kahlbaum and is labeled "*zur elem. analyse.*" There may be a certain selectivity in the decomposition of $PbO_2$ to PbO since only half of the oxygen is released, but, if so, we might expect it to favor the $O^{16}$ and make our ratio too high. Since the chief importance of this ratio lies in the fact that it is used to connect the chemical atomic weight scale with the isotopic scale where $O^{16}$ is taken to be 16.0000, it is important that the sample analyzed contain the same isotopic mixture that is most likely to occur in chemical compounds. We are planning to make other measurements, preparing our oxygen in other ways from different sources. Among these we hope to get a sample from the deep and aged rocks of the earth's crust. We also expect to make determinations of $O^{17}$.

We believe that in the method described all systematic sources of error have been eliminated except one. There is always the possibility of some unknown ion of mass 34 being present in small amounts. We would expect such an ion, if present, to fluctuate in intensity, relative to oxygen, under different discharge conditions. The fluctuations observed have never exceeded the errors of reading so we think the presence of such an ion improbable.

We wish to thank Mr. Pearson for his advice and to acknowledge the painstaking labor of Mr. Bressler in building this apparatus which was not put into operation until after his death.

[5] Aston, Nature **130**, 21 (1932).

[6] Mecke and Childs, Zeits. f. Physik **68**, 362 (1931).

[7] H. Kallman and W. Lasareff, Zeits. f. Physik **80**, 237 (1933).

# The Arc Spectrum of Osmium

WALTER ALBERTSON, *George Eastman Research Laboratory of Physics, Massachusetts Institute of Technology*

(Received January 11, 1934)

Over 1050 osmium lines have been classified as transitions between 137 terms of Os I. $J$ values have been assigned to all terms without the aid of Zeeman effect studies. If Hund theory is to apply to Os I then the $J$ assignment is unique. The classification is consistent as regards absorption lines, persistent lines, intensities, and comparison with analogous spectra. Comparison with iron shows that nearly all the terms from $d^6s^2$ and $d^7s$ found in Fe I have been found in Os I. The normal state of osmium is $5d^66s^2(^5D_4)$. The order of $J=2$ and $J=3$ is inverted in the four lowest "multiplets." Electron configurations and "multiplets" overlap to such an extent that the unambiguous assignments of $L$ and $S$ values and electron configurations are impossible for most terms. If the term assumed to be $5d^66s(^6D)7s\,^7D_4$ is correctly designated, then a simple series calculation gives 8.7 volts as an approximate value for the ionizing potential of osmium. New wave-length measurements to extend the analysis are to be made using a grating having a dispersion of 0.4A/mm in the second order. Evidence is presented to show that the normal electron configuration of iridium is $5d^76s^2$.

## INTRODUCTION

THE first regularities found in the spectrum of osmium were noted by C. P. Snyder in 1900, long before any theory of complex spectra had been developed. His results, however, were extremely meager, consisting of a constant difference wave number array of 6 columns and 13 rows, containing 55 lines. Snyder never published his work but sent it to Professor H. A. Rowland, who gave the array to Dr. N. E. Dorsey, his assistant, who later placed it in the hands of Dr. W. F. Meggers. The author obtained the loan of the original array through the courtesy of Dr. Meggers. The present communication gives the results of an extension of the term array to 137 terms, accounting for over 1050 lines.

The arc spectrum of osmium is extremely rich in lines, the wave-length list used in this work containing over 2200. The data were taken from Meggers[1] for the region 8645–4500A, and from Kayser,[2] and Exner and Haschek[3] for the region 4500–2251A. The region from 4280–3600 is somewhat incomplete due to overlapping of cyanogen bands. Meggers and Laporte[4] photographed the underwater spark spectrum, obtaining 193 lines in absorption between 4420A and 2211A. With these data they were able to establish the energies of the levels appearing in Snyder's array.

Zeeman effect observations for 32 lines have been published by Moore,[5] but these results are of such a qualitative nature as to be of no aid in establishing quantum numbers.

## PROCEDURE

The ordinary criteria used in classifying spectra, such as Zeeman effects, selection rules, interval rule, and intensities cannot be effectively applied to the elements of the third transition group. Not only is the coupling of an intermediate type, but different electron configurations of the same parity overlap to such an extent that strong perturbations enter to further distort the "multiplets."* In all but a few instances it will be quite impossible, and, in fact, quite meaningless to assign levels to electron configurations and values of $L$ and $S$ to the levels.

The inconvenience caused by the breakdown of the selection rules is partially compensated for

[1] Meggers, Sci. Papers Bur. Standards **20**, 35 (1924).
[2] Kayser, Astrophys. J. **7**, 181 (1898).
[3] Exner and Haschek, *Wellenlängen-Tabellen* (1904).
[4] Meggers and Laporte, Phys. Rev. **28**, 642 (1926).
[5] Moore, Astrophys. J. **28**, 1 (1908).

* Quotation marks are used to indicate that the word is not meant in the usual sense that applies when good $LS$ coupling is present. Rather, it is used here in intermediate coupling to indicate that group of levels which appear to be most closely associated with the levels of the true multiplet that would be present if the coupling were $LS$. See Bacher and Goudsmit—*Atomic Energy States*, paragraphs 6, 8 and 10.

by the larger number of combinations, and hence the increased effectiveness of the combination principle as the means of establishing a term array. Because Snyder's array is so fragmentary, it was decided to make an independent start, by using the mechanical interval recorder.[6] A selected group of the 184 strongest osmium lines were run through the machine. A glance at the record showed an unusual number of coincidences occurring at an interval of 1419.9 $cm^{-1}$; eight pairs of lines fitting to within 0.1 $cm^{-1}$. Additional pairs of lines which gave intervals corresponding to intervals between different sets of the eight pairs were obtained from the record; some of which established columns that gave several combinations with the rows previously established by the eight pairs. Continuing in this manner, an array of seven columns and twenty-nine rows was established in but a few hours.[7] The new array contained all of Snyder's array except the column at 3931.0 $cm^{-1}$, which later proved to be false.

The mechanical interval recorder was a great aid in the combing of the complete list of wave numbers with a given interval. A record for a large number of the lines was obtained so that for a given interval 1 mm on the record was equivalent to about 200 $cm^{-1}$. A scale was then made so that the wave number of one of the two lines which gave the interval in question could be read directly to within 100 $cm^{-1}$. This aid reduced the time to comb the wave-number list with a given interval by a factor of eight or ten.

Early in the work it was obvious that the terms fell into different groups as regards combinations. In most cases there is no ambiguity as to which combination, or $J$ group, the term belongs. Seven of these groups have been found.

The most satisfactory method of determining $J$ values is from the number of components into which a term is split in a magnetic field. Since no quantitative Zeeman effect data are on hand for osmium, other means of assigning $J$ values to the terms must be used. Fortunately, in this case the assignment can be done uniquely with only such criteria as the values of $J$ and the number of each expected from the different electron configurations. Any other assignment than the present one violates theory either by resulting in larger values than allowed by the electron configurations, or by giving negative $J$ values. Besides being uniquely assigned, the terms of given $J$ appear in the proper number and expected positions when analogy is made with iron. Most of the intense lines, persistent lines, and strongly absorbed lines are associated with the correct type of terms as expected from theory. However, in spite of this excellent agreement a further check on the $J$ value assignment by Zeeman effect is highly desirable.

## The Term System of Os I

The complete list of terms is given in Table I. The first column gives the term symbol used in this work. The quantum numbers assigned in this column are explained below. Column two gives the $J$ values of the term; column three, the energy of the term in $cm^{-1}$; column four, the number of combinations found for the term. Osmium is extremely rich in combinations, some of the leading low terms combining with more than 90 percent of the terms allowed by the $J$ selection rule. The term 2, for example, combines with 39 out of a possible 42.

The lowest terms of osmium are expected to arise from the electron configurations $5d^6 6s^2$ and $5d^7 6s$, the normal state of the atom being either $^5D_4$ from $5d^6 6s^2$ or $^5F_5$ from $5d^7 6s$. The former is found to be the normal state of osmium; the latter occurs at a position 5144.0 $cm^{-1}$ above the ground state.

Existing data[8] indicate that the term order of the elements in the third transition group should be more nearly similar to the corresponding elements in the first group, rather than to the ones in the second group. This is because the $d$ electrons are more tightly bound than the $s$ electrons in the second group in comparison with the first and third groups. For this reason the term systems of osmium and iron should show similarities. Fig. 1 shows that this is the case, especially among the very low terms. The broken lines in the figure connect iron and osmium terms which, in the opinion of the author are most nearly analogous. Electron configurations and "multi-

[6] Harrison, R.S.I. **3**, 753 (1932); **4**, 581 (1933).

[7] Albertson, Phys. Rev. **43**, 501 (1933).

[8] Bacher and Goudsmit, *Atomic Energy States*, McGraw-Hill (1932).

TABLE I. *Complete list of terms.*

| Term symbol | J value | cm⁻¹ | Number of combinations |
|---|---|---|---|
| 1 $d^6s^2\ ^5D$ | 4 | 0.0 | 34 |
| 2 $^5D$ | 2 | 2740.5 | 39 |
| 3 $^5D$ | 3 | 4159.4 | 46 |
| 4 $d^7s\ ^5F$ | 5 | 5144.0 | 34 |
| 5 $^5D$ | 1 | 5766.2 | 18 |
| 6 $^5D$ | 0 | 6092.9 | 6 |
| 7 $^5F$ | 4 | 8742.8 | 50 |
| 8 $^5F$ | 2 | 10165.9 | 35 |
| 9 $d^7s\ ^3F$ | 4 | 11030.6 | 47 |
| 10 $^5F$ | 3 | 11378.0 | 42 |
| 11 $^3F$ | 2 | 12774.3 | 31 |
| 12 $^5F$ | 1 | 13020.0 | 20 |
| 136 | 2 | 13364.8 | 23 |
| 13 $^3F$ | 3 | 14091.4 | 36 |
| 14 $^3H$ | 5 | 14339.0 | 27 |
| 15 $^3H$ | 4 | 14848.1 | 39 |
| 16 $^3H$ | 6 | 14852.4 | 13 |
| 17 | 2 | 15222.6 | 35 |
| 18 $d^7s\ ^5P$ | 3 | 15390.7 | 37 |
| 126 | 1 | 16212.4 | 16 |
| 19 | 1 | 17667.4 | 16 |
| 137 $^3P$ | 0 | 18301.4 | 4 |
| 20 | 3 | 18902.0 | 37 |
| 21 | 4 | 19108.9 | 35 |
| 22 | 2 | 19410.6 | 23 |
| 23? | 4 | 19759.9 | 10 |
| 24 | 4 | 19893.1 | 33 |
| 25 | 1 | 21033.5 | 12 |
| 124 | 2 | 21303.3 | 20 |
| 128 | 0, (1) | 22563.7 | 4 (6) |
| 26° $d^6sp\ ^7D°$ | 4 | 22615.8 | 11 |
| 125 | 2 | 23317.6 | 18 |
| 127 | 4 | 23322.7 | 19 |
| 27° $^7D°$ | 5 | 23463.0 | 9 |
| 28 | 5 | 24292.0 | 15 |
| 29° $^7D°$ | 3 | 25013.0 | 9 |
| 31° $^7D°$ | 2 | 25275.4 | 9 |
| 30 | 3, (4) | 25593.9 | 15 |
| 32° $d^6sp\ ^7P°$ | 4 | 28331.8 | 14 |
| 33° | 3 | 28371.7 | 17 |
| 34° $d^6sp\ ^7F°$ | 6 | 29099.4 | 4 |
| 35° | 3 | 29381.6 | 15 |
| 36° | 2 | 30078.3 | 14 |
| 37° | 5 | 30280.0 | 12 |
| 38° | 1 | 30524.9 | 10 |
| 39° | 4 | 30591.5 | 17 |
| 40° | 2 | 32457.4 | 15 |
| 41° | 4 | 32684.7 | 19 |
| 42° | 3 | 33124.5 | 22 |
| 43° | 3 | 34125.5 | 19 |
| 44° | 5 | 34365.3 | 14 |
| 45° | 4 | 34803.9 | 14 |
| 46° | 2 | 35090.5 | 17 |
| 47° | 3 | 35616.0 | 27 |
| 48° | 1 | 35919.5 | 16 |
| 49° ? | 1 | 36264.5 | 4 |
| 50° | 2 | 36345.9 | 15 |
| 51° | 2 | 36634.5 | 17 |
| 52° | 3 | 36806.3 | 19 |
| 53° | 5 | 36818.1 | 16 |
| 54° | 4 | 36826.2 | 18 |
| 55° | 3 | 37808.6 | 24 |
| 56° | 4 | 37908.8 | 16 |
| 57° | 2 | 37921.8 | 18 |
| 58° | 4 | 38130.1 | 19 |
| 59° | 1 | 38244.2 | 17 |
| 60° | 3 | 38264.1 | 22 |
| 61° | 2 | 38330.8 | 20 |
| 62° | 3 | 38485.9 | 20 |
| 63° | 1 | 38613.6 | 11 |
| 64° | 2 | 38741.3 | 16 |
| 65° | 2 | 38875 9 | 9 |
| 66° | 3 | 39383.0 | 16 |
| 67° | 5 | 39406.0 | 11 |
| 68° | 2 | 39493.8 | 13 |
| 69° | 2 | 39674.9 | 14 |
| 70° | 3 | 39772.3 | 7 |
| 71° | 4 | 40087.1 | 14 |
| 72° | 6 | 40290.6 | 5 |
| 73° | 4 | 40361.8 | 13 |
| 74° | 1 | 40497.5 | 10 |
| 75° | 2 | 40888.1 | 11 |
| 76° | 6 | 41023.2 | 5 |
| 77° | 5 | 41225.1 | 14 |
| 78° | 5 | 41725.6 | 11 |
| 79° ? | 6 | 41754.1 | 3 |
| 80° | 3 | 41875.9 | 18 |
| 81° | 5 | 42310.4 | 10 |
| 82° | 3 | 42316.8 | 13 |
| 129° | 1, (2) | 42422.3 | 8 |
| 83° | 4 | 42746.7 | 14 |
| 84° | 3 | 43011.4 | 16 |
| 85° | 5 | 43401.8 | 9 |
| 86° | 2 | 43437.0 | 12 |
| 87° | 3 | 43515.7 | 17 |
| 121° | 4 | 43754.7 | 9 |
| 88° | 4 | 43862.7 | 16 |
| 89° | 5 | 43876.2 | 7 |
| 90° | 2 | 44075.3 | 13 |
| 91° | 2 | 44662.8 | 10 |
| 92° | 4 | 44892.7 | 14 |
| 93° | 5 | 44921.2 | 7 |
| 94° | 2 | 45252.2 | 6 |
| 95° | 6 | 45315.9 | 3 |
| 96° | 3 | 45561.9 | 9 |
| 97° | 5 | 45758.9 | 7 |
| 98° | 3 | 46169.5 | 10 |
| 99° | 4 | 46263.5 | 12 |
| 100° | 4 | 46328.0 | 9 |
| 101° | 3 | 46776.3 | 15 |
| 120° | 3 | 47057.2 | 7 |
| 102° | 4 | 47158.4 | 9 |
| 103 $d^6s\cdot s\ ^7D$ | 5 | 47198.8 | 8 |
| 104° | 5 | 47200.2 | 5 |
| 105° | 3 | 47614.7 | 10 |
| 106° | 3 | 48302.6 | 10 |
| 107 $^7D$ | 4 | 48737.5 | 12 |
| 108° | 2 | 49112.0 | 9 |
| 133° ? | 5, (4) | 49534.2 | 4 |
| 109° | 3 | 49946.9 | 7 |
| 132° | 4 | 50293.9 | 9 |
| 135° | 5 | 50377.2 | 7 |
| 131° | 4 | 50937.3 | 8 |
| 110 $d^6s\cdot s\ ^5D$ | 4 | 51038.6 | 15 |
| 111 $^7D$ | 3 | 51138.2 | 15 |
| 130° | 5, (4) | 51152.0 | 8 |
| 112 | 2 | 52148.7 | 16 |
| 113 $^5D$ | 3 | 52401.9 | 21 |
| 134° | 4, (3) | 52534.6 | 5 |
| 114 | 2 | 53594.6 | 17 |
| 115 | 3 | 54676.9 | 19 |
| 116 | 3 | 55388.9 | 9 |
| 122 | 5 | 55402.6 | 12 |
| 117 | 4 | 55419.0 | 11 |
| 123 | 2 | 56092.5 | 8 |
| 118 | 5 | 56222.5 | 15 |
| 119 | 4 | 56729.2 | 17 |

plets" overlap to such an extent that this analogy cannot be carried too far. Since the $L$ and $S$ values assigned to certain terms in column one of Table I were all obtained in this manner, they should be considered only as a notation for stating that in the opinion of the author this osmium term with its $L$, $S$ and $J$ values more nearly resembles the corresponding iron term of same $L$, $S$ and $J$ value than does any other osmium term of the same $J$ value. Such statements can be made, since particular values of $L$ and $S$ do dominate a given term when the coupling is intermediate; although in certain instances the domination is by such a scant margin that the choice of particular values of $L$ and $S$ is a matter of personal opinion.[9]

One particular feature of the lower terms is the inversion of the expected order of $J=2$ and 3 in

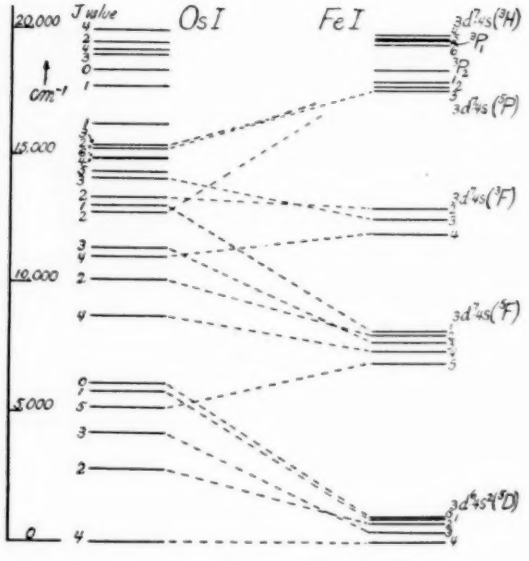


FIG. 1. Term systems of Os I and Fe I.

[9] Bacher and Goudsmit, *Atomic Energy States*. Paragraphs 6, 8 and 10.

the four "multiplets" $^5D$, $^5F$, $^3F$, $^5P$. All the other terms in these "multiplets" occur in the expected order.

The term 107 appears to be analogous to $d^6s \cdot s\ ^7D_4$ of iron. If such is the case, it can be used with the ground level to give a rough approximation of the ionization potential. The simple series calculation gives a value of about 8.7 volts.

Fig. 2 shows a plot of the wave-number separation of the lowest term of $d^{n-1}s^2$ from the lowest term of $d^{n-1}s$ for all the elements of the first long period (full line) and for those of the third period (broken line) for which data are available. The assignment given to osmium places its point in good agreement with its expected position. The two lowest terms in iridium are $J=9/2$ terms.[10] One is apparently the lowest term, $^4F_{9/2}$, from $d^7s^2$ and the other, the lowest term, also $^4F_{9/2}$, from $d^8s$. Omitting iridium from the plot for the moment, it is obvious where its point should go, and hence that $d^7s^2$ is the normal electron configuration of the atom.

It is of interest to note, as is shown in Table II, that all sensitive lines of osmium,[11] except one,

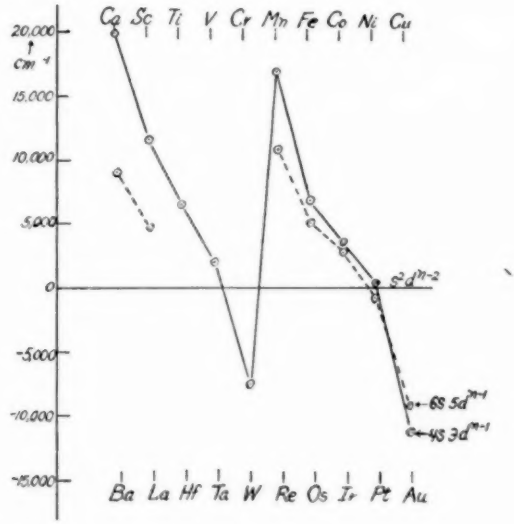


FIG. 2. Plot of the wave-number separation of the lowest term of $d^{n-1}s^2$ from the lowest term of $d^{n-1}s$ for all the elements of the first long period (full line) and for those of the third period (broken line) for which data are available.

[10] Albertson, Phys. Rev. **42**, 443 (1932).

[11] Twyman and Smith, *Wave-length Tables for Spectrum Analysis*. Adam Hilger, p. 128 (1931).

TABLE II. *Sensitive lines of osmium.*

| λI.A. | Int. | Combination | J Comb. |
|---|---|---|---|
| 4420.46 | 20*R* | 1—26° | 4—4 |
| 4260.85 | 20 | 1—27° | 4—5 |
| 3267.94 | 10*R* | 1—39° | 4—4 |
| 3262.30 | 8*R* | 3—45° | 3—4 |
| 3058.66 | 8*R* | 1—41° | 4—4 |
| 3030.70 | 4*R* | 4—58° | 5—4 |
| 3018.04 | 4*R* | 1—42° | 4—3 |
| 2909.08 | 8*R* (R.U.) | 1—44° | 4—5 |
| 2838.63 | 4*R* | 4—73° | 5—4 |
| 2637.12 | 3*R* | 1—56° | 4—4 |
| 2488.55 | 2*R* | 4—95° | 5—6 |

TABLE III. *Most strongly absorbed underwater spark lines of osmium.*

| λI.A. | I(abs.) | Comb. | λI.A. | I(abs.) | Comb. | λI.A. | I(abs.) | Comb. |
|---|---|---|---|---|---|---|---|---|
| 3301.55 | 25 | (1—37°) | 3018.05 | 10 | (1—42°) | 2320.20 | 7 | |
| 2909.07 | 25 | (1—44°) | 2838.64 | 10 | (4—73°) | 2289.32 | 7 | |
| | | | 2714.64 | 10 | (1—54°) | | | |
| 3058.66 | 20 | (1—41°) | 2689.80 | 10 | (4—81°) | 2919.83 | 6 | |
| | | (13—101°) | 2613.08 | 10 | (4—85°) | 2844.30 | 6 | (4—72°) |
| 2488.55 | 20 | (4—95°) | 2418.54 | 10 | (2—90°) | 2644.11 | 6 | (1—55°) |
| 2425.00 | 20 | (1—77°) | 2387.29 | 10 | (1—80°) | 2379.40 | 6 | (4—102°) |
| 2377.05 | 20 | (4—104°) | | | | 2308.32 | 6 | |
| 2270.18 | 20 | (2—101°) | 2370.69 | 10 | (3—100°) | | | |
| 2264.60 | 20 | (3—106°) | 2362.77 | 10 | (1—81°) | 3752.54 | 5 | (2—35°) |
| | | | 2303.32 | 10 | (1—85°) | 3232.07 | 5 | (3—46°) |
| 3267.94 | 15 | (1—39°) | | | | 3030.70 | 5 | (4—58°) |
| 2637.12 | 15 | (1—56°) | 2806.91 | 8 | (1—47°) | 2912.36 | 5 | (3—62°) |
| 2252.03 | 15 | (4—133°) | | | | 2860.97 | 5 | (4—71°) |
| | | | 2513.25 | 7 | (4—93°) | 2796.73 | 5 | (2—62°) |
| 3262.29 | 10 | (3—45°) | 2461.43 | 7 | (4—97°) | | | (9—101°) |
| 3156.24 | 10 | (4—53°) | 2324.25 | 7 | (1—84°) | 2786.31 | 5 | (4—76°) |
| 3040.90 | 10 | (2—47°) | | | | | | |

have either $d^6s^2(^4D_4)$ or $d^7s(^5F_5)$ for their lowest level. Also, as is shown in Table III, 27 of the 37 strongest absorption lines start from these same levels, while the rest start from $^4D_3$ or $^4D_2$. Nearly all the absorption lines listed by Meggers and Laporte[4] have been connected with the low terms below 13,000 cm$^{-1}$.

Because of lack of space and incompleteness of the classification, it is not thought worth while to publish the complete list of classified osmium lines at this time. However, Table IV contains a list of all the stronger lines, from intensity 30 to 6 inclusive on Exner and Haschek's scale. Only one of the 52 lines remains to be classified. The intensities are arc intensities, an *R* indicates reversed in underwater spark; a *P* that the line is a persistent line. The average deviation of experimental and calculated wave-lengths for lines in the complete list is slightly less than ±0.01A, which is well within the experimental error of Kayser and Exner and Haschek's measurements. The agreement for the lines measured by Meggers is even better, except in the infrared.

TABLE IV. *All strongest lines in Os arc from I=30 to I=6 inc.*

All intensities are from Exner and Haschek's estimates.

| λI.A. Int. | Comb. | λI.A.° Int. | Comb. | λI.A. Int. | Comb. |
|---|---|---|---|---|---|
| 4135.81—30 | (3—32°) | 3656.90—10 | (2—36°) | 3058.68— 8*RP*** | (1—41°) |
| | (13—60°) | 3670.90—10 | (9—60°) | | (13—101°) |
| 4211.90—30* | (27°—103) | 3719.49—10 | (9—56°) | 3156.25— 8 *R* | (4—53°) |
| | | | (15—78°) | 3232.06— 8 *R* | (3—46°) |
| 3752.54—20 *R* | (2—35°) | 3720.12—10 | (7—47°) | 3262.30— 8 *RP* | (3—45°) |
| 3782.19—20 *R* | (3—39°) | | (16—78°) | 3336.16— 8 *R* | (3—43°) |
| 4112.04—20* | (5—36°) | | (31°—112) | 3370.58— 8 *R* | (4—45°) |
| 4260.85—20 *P* | (1—27°) | | | 3532.83— 8 | (3—40°) |
| 4420.47—20 *RP* | (1—26°) | 3790.14—10 | (15—77°) | 3616.58— 8 | (8—55°) |
| | | 3836.03—10 | (7—45°) | 3640.35— 8 | (15—81°) |
| 3793.93—15 | (20—94°) | 3840.29—10 | | 4172.58— 8 | (8—43°) |
| 3963.65—15 | (3—35°) | 3849.96—10 | (11—64°) | 4189.91— 8 | (11—51°) |
| 3977.24—15 | (4—37°) | 3857.09—10 | (3—36°) | | |
| 4173.24—15 | (4—34°) | 3876.76—10 | (9—53°) | 4328.69— 8 | (9—43°) |
| | | 4066.70—10 | (26°—103) | 4394.88— 8 | (10—43°) |
| 3267.96—10 *RP* | (1—39°) | 4091.84—10 | (6—38°) | | |
| 3301.56—10 *R**** | (1—37°) | 4175.62—10 | (7—41°) | 3387.86— 6 | (8—69°) |
| 3528.60—10 *R* | (1—32°) | 4293.98—10 | (15—58°) | 3401.87— 6 | (7—58°) |
| 3559.82—10 | (7—54°) | 4311.41—10 | (4—32°) | 3402.52— 6 | (1—35°) |
| 3560.88—10 *R* | (7—53°) | | | 3504.66— 6 | (3—41°) |
| 3598.10—10 | (2—38°) | 2909.09— 8*RP* | (1—44°) | 3865.44— 6 | (31°—111) |
| | (13—80°) | | | 3938.59— 6 | (7—43°) |

* Kayser gives 4211.90—30 and 4112.04—20 only moderate intensities.

** 3058.68—8*RP* is listed as one of the second strongest Os arc lines by Kayser.

*** 3301.56—10*R* is listed as the strongest Os arc line by Kayser.

## CONCLUSION

It is thought advisable to obtain a new and better description of the arc spectrum of osmium before continuing with the classification. In many instances the estimated intensities as given separately by Kayser and by Exner and Haschek are not in good agreement. The region between 3800A and 3600A has never been completely photographed. Comparison between arc and spark spectra from the existing tables allows for the elimination of only a very few of the spark lines. No doubt many of the weaker unclassified lines in the arc list will later prove to be spark lines. Much is to be desired in the way of better wave-length measurements, principally because so much must be done solely by the combination principle. Surely, some of the lines will be shown to be erroneously classified when more accurate wave-lengths are at hand, and some few of the weaker ones may prove to be spark lines. Finally, Zeeman effect measurements should be obtained to check the $J$ value assignment and for any other data that they might yield.

All the above will be undertaken in the Spectroscopy Laboratory at M. I. T. in the near future. The wave-lengths will be measured with plates taken from the large 35 ft. 180,000 line grating, having a dispersion of 0.4A mm in the second order. Preliminary measurements of the wave-lengths of iridium, with this grating, indicate that for sharp lines the accuracy of measurement is limited only by the accuracy of the iron standards.

I wish to thank Professor G. R. Harrison, in whose laboratory this work was done, and Professor H. N. Russell of Princeton for his interest and criticism during the course of the work.

# Study of Ionization in Nitrogen at High Pressures

S. CHYLINSKI, *University of Chicago*

(Received December 13, 1933)

The ionization-pressure relation in nitrogen has been studied at various pressures up to about 120 atmospheres. This was done for both gamma- and residual- (=local+wall +cosmic radiations) rays with and without a lead shield. The resulting curves seem to have identical forms. The ratios of gamma to residual ionizations are constant for pressures down to about 20 atmospheres, decreasing rapidly for lower pressures. A series of saturation characteristics of nitrogen at various high pressures (up to about 109 atm.) and intensities ranging from about 7 to 1200 ions per cc per sec. per atm. were also determined experimentally. These characteristics do not have identical forms, i.e., they cannot be made to coincide if multiplied by constant factors.

A STUDY of the residual ionization in nitrogen has been made by Broxon[1] who found that it was greater than that in air at corresponding pressures; also, that the ionization per atmosphere decreased with pressure and that the ionization-pressure characteristic became practically horizontal for pressures greater than 100 atmospheres. Outside of some earlier work which is referred to in Broxon's paper the only other experiment on the ionization of nitrogen was an incidental test by Compton, Bennett and Stearns[2] who found that the ionization in nitrogen at 100 atmospheres due to gamma-rays was about 25 percent greater than in air.

## APPARATUS

A diagram of the apparatus is shown in Fig. 1. The cylindrical ionization chamber, of inside dimensions $2\frac{1}{4}$ by 12 in., was made of seamless steel tubing of $\frac{3}{8}$ in. wall thickness. The shield consisted of a lead cylinder, 1.5 in. thick, which was cast in two parts. The ends were removable lead disks.

The collecting electrode, a $\frac{1}{16}$ in. steel rod, conducts the ionization current to the Lindemann electrometer $E$ which, outside of its own housing, has no other shield. An amber cone, through which this electrode passes, insulates it from the rest of the apparatus. The guard ring system is so designed that it not only prevents actual conduction of electricity to the insulated system, but also acts as an effective shield against induction disturbances on the electrode from the hard rubber, which separates the guard ring from the steel cylinder.

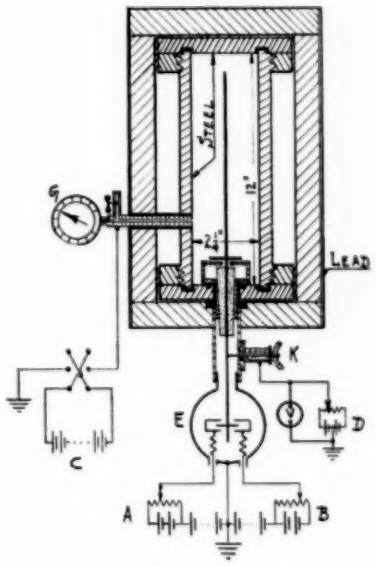


FIG. 1. Diagram of apparatus and electrical connections.

The grounding key $K$ was screwed into a short piece of brass tubing which was a part of the guard system. This brass tubing supported the electrometer, the connection being made practically air tight by a rubber gasket. The connect-

[1] J. W. Broxon, Phys. Rev. **38**, 1704 (1931).
[2] A. H. Compton, R. D. Bennett and J. C. Stearns, Phys. Rev. **39**, 873 (1932).

ing passage was at atmospheric pressure and was dried with a $P_2O_5$ tube, as was also the electrometer.

The apparatus was set up in the basement of Eckhart Hall with the long axis of the ionization chamber in a vertical position. The center of the chamber was roughly 5 ft. from both floor and ceiling, about 6 ft. from either side wall and 2 ft. from the front wall. The rear wall was 15 ft. away. As a source of gamma-rays, 1 mg of radium was used. This was sealed in a glass capsule which was placed into a lead cylinder so that about 1 cm of lead surrounded the radium. When in use the radium was suspended from some gas pipes so that its distance from the ceiling was about 2 ft., along the axis of the ionization chamber. In some cases it was placed directly on top of the chamber.

To determine the absolute magnitude of the ionization currents the capacity of the system had to be known. For this purpose two standard cylindrical condensers could be screwed in place of the grounding key. The capacity of the apparatus was computed to be 18.29 cm with a probable error of 1.5 percent. The sensitivity of the electrometer throughout this work, with the exception of the two highest intensities, was about 100 divisions per volt when using a 16 mm objective. The volume of the ionization chamber, experimentally determined, was found to be 780 cc.

## Ionization-Pressure Curves

These curves were taken with and without the lead shield, first with the radium 1 m away and then so far removed that its effect was practically negligible. The results for gamma-rays are given in Fig. 2 and for the residual radiation in Fig. 3. In those figures the curves marked I refer to results with the lead shield removed, while those marked II were taken with the lead shield in place. The ionization current values due to gamma-rays alone ($I_G$) were obtained by subtracting from the observed values the corresponding ionization currents due to the residual radiation alone ($I_R$).

The nitrogen used was of commercial quality. It had been stored for about four months before use so that one might reasonably assume that any radioactive contamination originally present had during that time decayed to negligible values. A day or so was allowed to elapse after filling before any ionization readings were taken. It was found that the value of the ionization current on fresh filling was considerably below the final steady value which was gradually reached in the course of a day. The reason for this effect is not clear though one is tempted to say that it is probably connected with the way in which the gas has been stirred in the process of filling. The

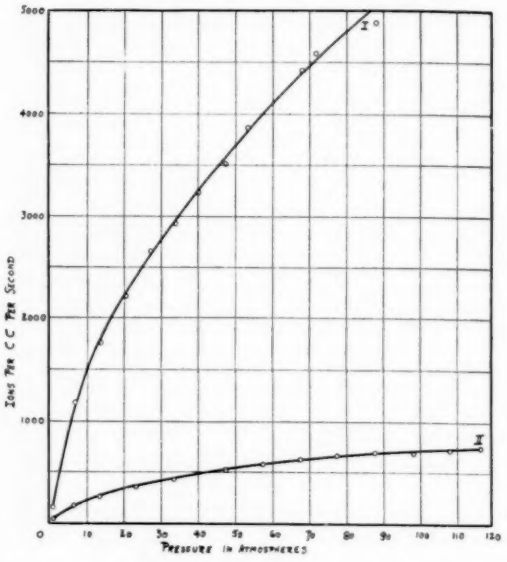


Fig. 2. Ionization-pressure characteristics of nitrogen due to gamma-rays. Curve I, lead shield off; curve II, lead shield in place.

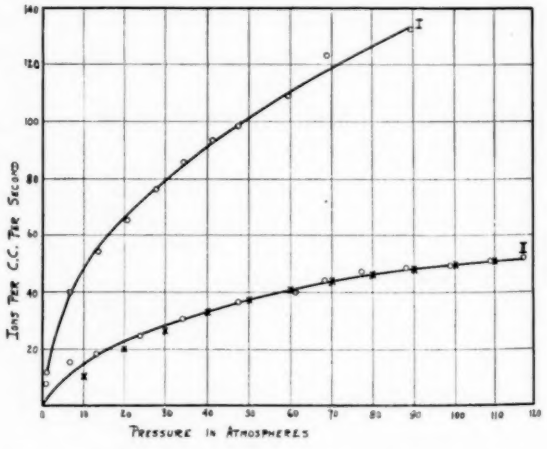


Fig. 3. Ionization-pressure characteristics of nitrogen due to residual-rays. Curve I, lead shield off; curve II, lead shield in place. Crosses refer to Broxon's results.

pressures were then decreased in steps of about six to ten atmospheres and again some time, usually about two to four hours, was allowed to elapse before recording. Alternate readings, with + and −180 volts on the chamber, were taken of the ionization currents, usually four of each type. In this way corrections for small electrical leaks were largely compensated. It is true that with this method spurious effects due to uncontrollable fluctuations of battery voltages are not corrected but experience showed that with reasonable care the results were reproducible even months apart.

The general form of these curves conforms well with those obtained by other observers for different gases. There is no indication of any possible maximum, a result first obtained and later disproved in the case of nitrogen. Erikson's observations[3] on gamma-rays should be comparable with those of the author, yet no maximum was observed as in Erikson's case. The maxima might, of course, be very broad but on examining Erikson's paper one sees that his maxima fall within well-defined limits which should be within the region here investigated.

The crosses in curve II of Fig. 3 have been drawn to facilitate a comparison with Broxon's results.[1] His absolute values lie about 18 percent higher than those here recorded. In order to compare the forms of the two curves, Broxon's results for each pressure were multiplied by the factor 0.819, that being the ratio of the ordinates of the two curves for the highest pressure used in this work. It is seen that from about 30 atm. on the agreement is almost perfect while below that pressure there is a gradually increasing difference with decreasing pressures. A possible explanation may be that the author's ionization chamber had some radioactive contamination in the walls, an explanation which seems to be borne out by the smaller ratios of gamma to residual ionizations obtained at the lower pressures, a point which is brought out below.

The curves have identical forms. Multiplying the ordinates of curve I by the ratio of the ordinates of II and I at the highest pressure, one obtains points which lie quite accurately on curve II.

It is significant that no saturation values were obtained even at the highest pressures. The rise in ionization even at 120 atm., although comparatively small, is not negligible. In this the results of these experiments agree with those of practically all observers with the exception of Erikson.

The ratios of the gamma-ray ionization $I_G$ to the residual ionization $I_R$ at corresponding pressures are shown in Fig. 4. Curve I in that figure

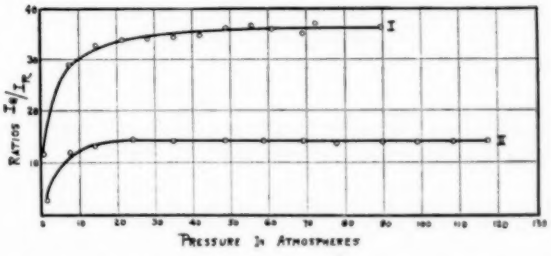


FIG. 4. Ratios of gamma-ray ionization $I_G$ to residual-ray ionization $I_R$ at various pressures of nitrogen. Curve I, lead shield off; curve II, lead shield in place.

represents the values when no shield was used and curve II represents the values with the lead shield in place. Below about 20 atm. the values of the ratios in both curves decrease rapidly with decreasing pressures. As stated above, the smaller ratios at the lower pressures might possibly be explained, as pointed out by Broxon, by assuming the existence of a small contamination in the chamber walls which becomes decreasingly effective with higher pressures, of the type described by Millikan.[4] The points of curve II lie much smoother than those of curve I. The explanation of this probably lies in the fact that when the shield is used, disturbances, such as x-rays in the laboratory, are without effect upon the ionization. From what has been said above one would expect that if curve II were "multiplied" to make it lie in the same region as curve I, the two curves should coincide. However, a glance shows that that is only approximately true; at the higher pressures, curve II is more nearly horizontal than curve I. Still, although nothing definite can be said about these ratios until the effect of wall radiation is known, it is of interest to note the similarity at the higher pressures.

[3] Erikson, Phys. Rev. [1] **27**, 473 (1908).

[4] R. A. Millikan, Phys. Rev. **39**, 397 (1932).

## Saturation Curves for Nitrogen at Various High Pressures and Intensities

The data for the different intensities were taken with the radium capsule located at different distances from the center of the ionization chamber along its axis. The pressure was 109 atm. The voltages, applied between the needle and chamber, ranged from 4 to about 200 volts. After each reversal of voltage, as well as after each increase, care was taken so that during the readings steady conditions prevailed.

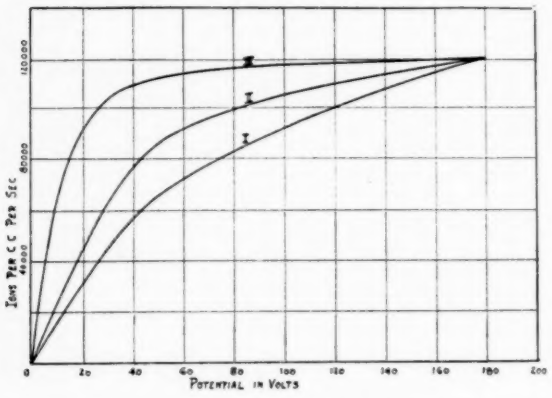


Fig. 5. Saturation characteristics of nitrogen at various pressures. Pressure of 109 atm., and various intensities. Curve I, radium capsule placed on top of chamber with top end of lead shield removed; curve II, radium capsule placed directly on top end of lead shield; curve III, radium 1 m from center of chamber along its axis. Lead shield in place.

The results are shown in Fig 5. For convenience of comparison the ordinates of the original saturation curves have been multiplied by factors so as to make them coincide for the ordinate value of 180 volts. Curves I, II and III represent respectively the original values multiplied by the factors 1, 4.57 and 165. These curves show graphically that the form of the saturation curves is a function of the ionization intensities. Hopfield[5] reaches similar conclusions from his recent work in contradiction to Bowen[6] whose work shows that the form of the saturation curves is independent of ionization intensities. One must keep in mind, however, that Bowen worked with considerably smaller intensities of ionization (of the order of 30 ions per cc per sec. per atm. for the high intensities and about one-fifth that amount for the low); also, that he was able to use high saturation voltages. His ionization chamber was so constructed that the ions were collected between parallel plates, thus making possible a high uniform field. Bowen's results for air at 93 atm. show that the form of the curves is independent of the intensity for potential gradients in the chamber from about 23 to 1000 volts per cm whereas for smaller gradients the independence appears questionable. The potential distribution in the author's ionization chamber was such as to make his results comparable with those of Bowen only in the case of the smaller gradients; for a simple computation shows that the potential drop from the central electrode to cylindrical surfaces concentric with it, for 180 volts applied between the electrodes of the chamber, is 131 volts for a surface of 1 cm radius, 32 volts for one of 2 cm radius and 16 volts for the remainder. This shows that most of the volume of the chamber has a small potential gradient. Apparatus of Bowen's type seems more suitable for further investigation of this part of the problem than either Hopfield's or the author's.

In the simple form of the saturation theory one assumes that there is a homogeneous spatial distribution of the strength of the ionization. This is probably sufficiently true when the ionizers are x-rays, or gamma-rays but cannot be true with alpha-particles. Results obtained with the latter led Langevin to the introduction of the idea of "columnar ionization" according to which cylindrical columns of very small cross section

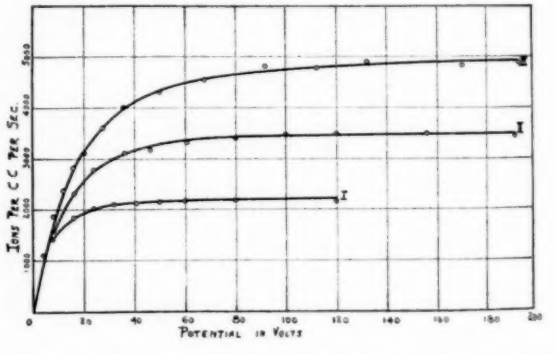


Fig. 6. Saturation characteristics of nitrogen at various pressures with radium capsule 1 m from center of ionization chamber and top end of lead shield removed. Curve I, pressure 27.25 atm; curve II, pressure 54.5 atm.; curve III, pressure 109.0 atm.

[5] John J. Hopfield, Phys. Rev. **43**, 675 (1933).
[6] I. S. Bowen, Phys. Rev. **41**, 25 (1932).

and very large ion density are formed in the direction of the rays while the adjoining spaces have no ions. It is easy to see that in such a case the ion loss through recombination must be greater than with a uniform distribution of the ions and that therefore much higher field strengths are necessary to obtain a given degree of saturation. Hopfield[5] uses the idea of "columnar ionization" to explain some results of his recent work with gamma-rays. In view of the crooked nature of beta-ray tracks this assumption seems of doubtful value but at any rate it is subject to experimental test. For it at once leads to the conclusion that at a given voltage a higher degree of saturation should be obtained when the potential gradient is at right angles to the tracks than when it is parallel to them because in the first case there is a lateral displacement of the ions which should result in a better or more uniform distribution in the ionization chamber while in the second case the displacement is merely along the tracks and should therefore be of little effect upon the recombination. To check this point the cylindrical radium capsule was placed parallel to the axis of the chamber at such a distance from its center that the resulting ionization current at a given potential was just the same in magnitude as when the radium was placed along the axis of the chamber and for the same potential gradient. This was done at a pressure of 109 atm. and the resultant saturation curves were practically coincident within experimental error. Although it is realized that the apparatus did not lend itself to an accurate test of this point, yet, if there were pronounced columnar ionization, this test should have shown it up.

In Fig. 6 are shown the saturation curves at three different pressures. These curves reveal nothing of particular interest but it is well to include them in this study.

In conclusion I wish to express my gratitude to Professor Arthur H. Compton for permission to do this work in his laboratory and for valuable criticisms of the manuscript.

# The Distribution of Initial Velocities of Positive Ions from Tungsten

GEORGE J. MUELLER, *Cornell University, Ithaca, New York*

(Received December 4, 1934)

The distribution of initial velocities of positive ions emitted from a hot tungsten filament in vacuum has been investigated by measuring the positive ion current from a short length (0.05 cm) of filament to a coaxial cylindrical electrode against various retarding potentials. Measurements were made for eighteen different temperatures ranging from 1300°K to 3000°K. The ion current consisted of not only tungsten ions but also those of impurities, chiefly potassium. Within experimental error, it was found that the ions were emitted with velocities distributed in accordance with Maxwell's law.

## INTRODUCTION

THE distribution of the initial velocities of charged particles emitted from hot metals has been studied by a number of investigators. The pioneer experiments of O. W. Richardson and F. C. Brown[1, 2, 3] upon the initial velocity distribution of thermionic electrons were followed by the work of Schottky[4] and that of Ting,[5] Jones,[6] Potter,[7] Rössiger,[8] Congdon[9] and Germer.[10] Their experiments, especially those of Germer, show conclusively that the thermionic electrons emitted from hot metals into a high vacuum have a Maxwellian distribution of velocities.

O. W. Richardson[2] and F. C. Brown[11, 12] extended the work to include positively charged particles and examined a large number of substances. Their experiments were made at relatively low temperatures (below 1200°K) and because of the experimental technique used it was not possible to conclude with certainty that the distribution of energy was Maxwellian. In fact, Schottky[4] presented some evidence that the ions had greater energy than those found by Brown.

The ions used by Richardson and Brown in their experiments were those of impurities in the metal. Since then, Jenkins[13] and L. P. Smith[14] have discovered that at higher temperatures, ions characteristic of the metal itself were emitted. These ions have been studied by Smith,[15] H. B. Wahlin[16, 17] and L. L. Barnes.[18]

Smith[15] suggested that tungsten might slowly recrystallize in an irreversible manner at high temperatures liberating ions as a secondary effect, in which case the ions might not have a Maxwellian distribution of velocities. In view of this and the inconclusive nature of the work mentioned above, it was decided to investigate the velocity distribution of positive ions from hot tungsten.

## METHOD

The experiment consists of measuring the positive ion current flowing from a hot tungsten filament to a coaxial cylindrical electrode against various retarding potentials for definite filament temperatures.

If electrons leave the filament with their velocities distributed according to Maxwell's

[1] Richardson and Brown, Phil. Mag. **16**, 353 (1908).
[2] Richardson, Phil. Mag. **16**, 890 (1908).
[3] Richardson, Phil. Mag. **18**, 681 (1909).
[4] Schottky, Ann. d. Physik **44**, 1011 (1914).
[5] Ting, Proc. Roy. Soc. **A98**, 374 (1920–21).
[6] Jones, Proc. Roy. Soc. **A102**, 734 (1923).
[7] Potter, Phil. Mag. **46**, 768 (1923).
[8] Rössiger, Zeits. f. Physik **19**, 167 (1923).
[9] Congdon, Phil. Mag. **47**, 458 (1924).
[10] Germer, Phys. Rev. **25**, 795 (1925).
[11] Brown, Phil. Mag. **17**, 355 (1909).
[12] Brown, Phil. Mag. **18**, 649 (1909).
[13] Jenkins, Phil. Mag. **47**, 1025 (1924).
[14] Smith, Phys. Rev. **33**, 279 (1929).
[15] Smith, Phys. Rev. **35**, 381 (1930).
[16] Wahlin, Phys. Rev. **34**, 164 (1929).
[17] Wahlin, Phys. Rev. **37**, 467 (1931).
[18] Barnes, Phys. Rev. **42**, 487 (1932).

law, Schottky[4] has shown that for an infinitely long cylindrical arrangement of this kind, the relation between the current $i$ reaching the collector and the retarding potential $V$ is,

$$i=i_0\frac{2}{\pi^{\frac{1}{2}}}\left[(Ve/kT)^{\frac{1}{2}}\epsilon^{-Ve/kT}+\int_{(Ve/kT)^{\frac{1}{2}}}^{\infty}\epsilon^{-x^2}dx\right], \quad (1)$$

where $i_0$ is the saturation current, $e$ the charge on the electron, $k$ the Boltzmann constant and $T$ the temperature of the filament in degrees Kelvin. The sign of $V$ is chosen positive for retarding voltages applied between collector and filament. This expression will also hold in the case of positive ions, where $e$ is now the charge on the ion, and the sign of $V$ is again chosen positive for retarding voltages. In the calculation of Eq. (1), it has been assumed that the diameter of the filament is small as compared with the diameter of the collector, and that the current is not limited by space charge. C. Davisson[19] has discussed the limiting conditions due to space charge.

The relation between $\log_{10}(i_0/i)$ and $Ve/kT$ is approximately linear except in those cases where $(Ve/kT)<6$. Thus, it is convenient to plot the $\log_{10} i$ *vs.* $V$ from Eq. (1) corresponding to the temperatures used and see if the experimental points fall on the resulting curves.

## The Experimental Tube

The disturbing effect of electrons from the filament had to be eliminated. With the simple arrangement of a straight filament surrounded by a collecting cylinder, the measured current includes, in addition to the positive ions reaching the collector against the retarding potential $V$, the thermionic electrons from the filament and photoelectrons from various metal parts of the tube due to light from the filament. Of these, the thermionic electrons greatly exceed in number the positive ions. To prevent thermionic electrons from ever reaching the collector, an arrangement of concentric cylinders and applied potentials was used. As shown in Fig. 1, the filament $F$ coincides with the axis of nickel cylinders $A_1$ and $A_2$ carrying flanges $D_1$ and $D_2$ separated 0.05 cm. This serves to expose a short length of filament $\delta$ to the collecting cylinder $C$.

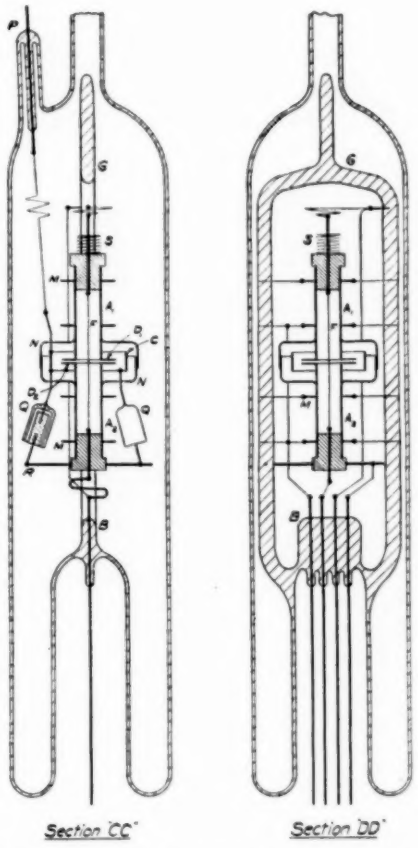


FIG. 1. Construction of the experimental tube (section $CC$ is taken at right angles to $DD$).

During the experiments, cylinder $A$ was made sufficiently negative (about twelve volts) with respect to the filament to produce saturation of the ion current and at the same time prevent thermionic electrons from reaching $C$. The retarding potential $V$ was applied between the collector $C$ and the filament $F$. Thus, although the ions are first accelerated and finally retarded, they effectively experience a retarding potential $V$.

It was established that no photoelectrons from the flanges reached the collector, for with an increase in $V$ no reversal of the collector current was detected.

With this arrangement of cylindrical electrodes, the fields are essentially radial and consequently Eq. (1) would hold if the filament $F$ were a unipotential surface. However, the

[19] Davisson, Phys. Rev. **25**, 808 (1925).

exposed length of filament was chosen so small that its effect was negligible as was shown by a mathematical analysis.

Cross sections of the assembled experimental tube are shown in Fig. 1. The filament is of tungsten $1.74\times10^{-2}$ cm (7 mil) in diameter and 5.7 cm long. It is supported vertically by lavite plugs and held taut along the axis of the nickel cylinder $A$ of diameter 0.792 cm and length 7.6 cm by a molybdenum spring $S$. The two flanges of outside diameter 2.38 cm were silver soldered to cylinders $A_1$ and $A_2$. The outside cylinder $C$, 2.86 cm in diameter and 0.79 cm long, was supported by three quartz insulators $Q$ from a ring of tungsten wire $R$ embedded in the glass framework $G$. All cylinders were made of 10 mil nickel sheet, butt jointed and silver soldered. In addition, cylinders $A_1$ and $A_2$ were reinforced with 15 mil nickel rings $M$. The shield $N$, consisted of two cups spun from sheet nickel, connected to and supported by cylinder $A$, completely surrounded cylinder $C$. The supports and electrical connection to $C$ passed through holes cut in $N$. The electrical lead from $C$ then passed through a special seal $P$. Leads to cylinder $A$, tungsten ring $R$, and the filament left the tube through the large press-seal $B$.

All metal parts were heated in an atmosphere of hydrogen, before being placed in the tube, to free them of oxides and other contaminations. The tube was then assembled and remained on the vacuum system during the entire experiment. Proper heat treatment was given the metal parts with an induction furnace, and the tube was baked out at 475°C for six hours before any measurements were made. The gas pressure was always less than $10^{-6}$ mm of mercury as shown by a McLeod gauge and an ionization gauge. The filament was not flashed, since the ions emitted at low temperatures (1300°K) were to be measured. The procedure was to bring the filament up to some desired temperature and age it at that temperature until the positive ion current reached a steady value, after which observations were made for various retarding potentials.

## The Current Measuring System

The current measuring system attached to the collecting cylinder is shown in Fig. 2. It consists

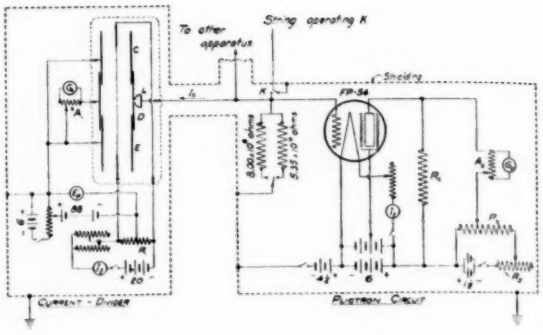


FIG. 2. The current measuring system.

essentially of a current-dividing tube as described by L. P. Smith[20] and a FP-54 Pliotron with its necessary controls. The current-divider was designed to deliver a small negative current $I_1$ which when balanced against the positive ion current $I_2$ from the experimental tube was indicated by a zero reading of the galvanometer in the plate lead of the Pliotron tube. The Pliotron with its associated circuit was also used to calibrate the current-dividing tube.

The maximum stable sensitivity of the Pliotron circuit was 60,000 mm per volt, allowing ion currents in the range $10^{-16}$ to $10^{-10}$ ampere to be measured. The entire measuring system, with the exception of the filament battery and the control rheostats of the current-dividing tube, was completely shielded. A brass box containing the FP-54 tube was made air tight and arranged in a manner such that dry air could be passed through the chamber to prevent electrical leakage.

## The Essential Circuit

A diagram of the essential circuit is given in Fig. 3. The tube filaments were heated by large capacity storage batteries, $V_1$ and $V_3$. The current flowing through the experimental filament was accurately determined by measuring the drop across a standard 0.1 ohm with a Wolff potentiometer. The position of the slider on the potentiometer $R_2$ was accurately adjusted so that a reversal of the filament current produced no effect on the positive ion current. $V_4$ and $V_5$, two twelve volt storage batteries, supplied the necessary accelerating and retarding

[20] Smith, Rev. Sci. Inst. **2**, 237 (1931).

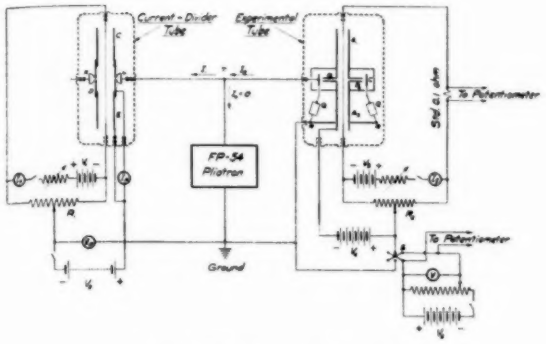


FIG. 3. The essential circuit.

potentials. The tungsten ring $R$, supporting the quartz insulators $Q$, was grounded to eliminate leakage across the insulators.

Both the current-dividing tube and the experimental tube were placed in a large metal box in which was placed a quantity of calcium chloride to reduce electrical leakage due to moisture. Guard rings were placed on all the special glass leads from the tubes. Leakage over the inner surfaces was eliminated by proper spacing in the design of the tubes.

## PROCEDURE

The positive ion current to cylinder $C$, for a given retarding potential and filament temperature, was balanced by an electron current of known magnitude thus insuring that the potential of $C$ remained constant. This was accomplished by increasing the temperature of the filament in the current-divider until the flow of electrons to its Faraday collector just neutralized the positive charge on electrode $C$ of the experimental tube as indicated by a zero reading of the galvanometer in the Pliotron circuit. With this null method a flow of positive ion current of $10^{-16}$ ampere could be detected. This balance, after some practice, could be attained with little effort. Such a method was found very reliable since the calibration of the current-dividing tube did not change over a period of two months.

The temperature of the filament in the experimental tube was determined from the diameter and the heating current, using the temperature characteristics of tungsten given by H. A. Jones and I. Langmuir.[21] The heating current was checked at the start and at the end of each set of measurements.

## EXPERIMENTAL RESULTS

Some of the various sets of measurements are shown graphically in Figs. 4 and 5. The curves show the theoretical values of $\log_{10} i$ as calculated from Eq. (1) with the use of observed

[21] Jones and Langmuir, Gen. Elec. Rev. p. 310, June, 1927.

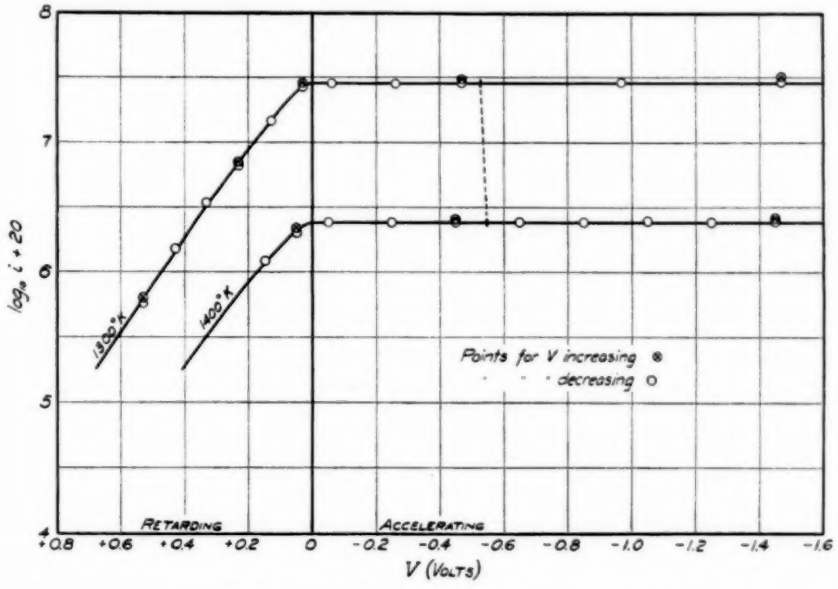


FIG. 4. Current-voltage data for low temperatures.

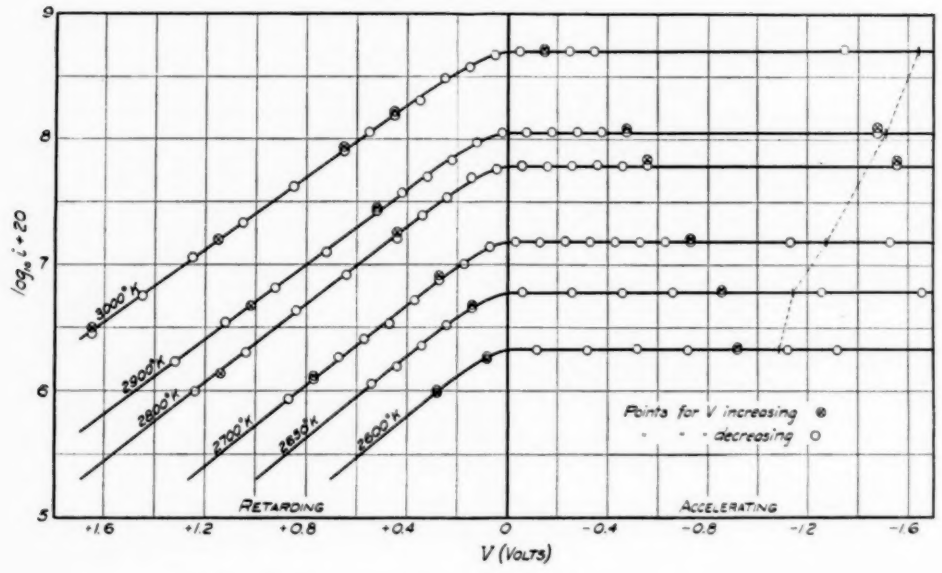


FIG. 5. Current-voltage data for high temperatures.

values of saturation current and temperature. The points indicate the observed values of $\log_{10} i$ after making a correction for the contact difference of potential between the collector and the filament. This correction may be illustrated by the data for $T=1300°K$. The observed points gave a curve which broke sharply at $V=-0.53$ and $\log_{10} i=7.45-20$. This value was taken for $\log_{10} i_0$ and the contact potential of the filament relative to the cylinder as + 0.53 volt. Such a correction was necessary for each set of observations since the contact difference of potential increased with temperature. The magnitude of $V$ at the intersections of the dashed line and the various curves gives the contact potential differences.

In taking points, the curves were traced twice, once for increasing values of retarding potential and then immediately for decreasing values of retarding potential ending at −12 volts. Germer experienced some difficulty in obtaining values of $\log_{10} i_0$ and of contact differences of potential at the higher temperatures due to space charge effects. No such difficulty was encountered in the present investigation since the current density was extremely low. Not all of the results are shown in the figures, but only representative sets of data. The first ions detected were those emitted at 1300°K. Mass-spectrograph studies of tungsten filaments made in this laboratory and elsewhere have shown that these low temperature ions are due chiefly to potassium found as an impurity in the tungsten. This emission disappeared above 1500°K. The next ions detectable were those given off at 2300°K. These were, very likely, a mixture of the ions of tungsten as well as those of impurities. It would, of course, be desirable to study the ions of tungsten alone, but present mass-spectrograph

TABLE I. *Summary of data.*

| Order | Filament | Heating current (amp.) | $T$ (°K) | $\log_{10} i_0+20$ | Contact diff. of potential (volts) |
|---|---|---|---|---|---|
| 7 | 2 | 1.00 | 1300 | 7.45 | +0.53 |
| 8 | 2 | 1.15 | 1400 | 6.38 | 0.55 |
| 9 | 2 | 1.32 | 1500 | 6.29 | 0.58 |
| 1 | 1 | 3.00 | 2300 | 6.33 | 0.79 |
| 2 | 1 | 3.11 | 2350 | 6.40 | 0.83 |
| 3 | 1 | 3.25 | 2400 | 6.47 | 0.89 |
| 4 | 1 | 3.36 | 2450 | 7.51 | 0.96 |
| 5 | 1 | 3.47 | 2500 | 7.69 | 1.02 |
| 6 | 1 | 3.60 | 2550 | 7.85 | 1.06 |
| 10 | 2 | 3.70 | 2600 | 6.33 | 1.08 |
| 11 | 2 | 3.82 | 2650 | 6.78 | 1.14 |
| 12 | 2 | 3.95 | 2700 | 7.18 | 1.27 |
| 13 | 2 | 4.10 | 2750 | 7.60 | 1.39 |
| 14 | 2 | 4.23 | 2800 | 7.78 | 1.44 |
| 15 | 2 | 4.35 | 2850 | 7.90 | 1.48 |
| 16 | 2 | 4.50 | 2900 | 8.05 | 1.52 |
| 17 | 2 | 4.62 | 2950 | 8.17 | 1.55 |
| 18 | 2 | 4.75 | 3000 | 8.69 | 1.65 |

studies made in this laboratory by A. Fogelsanger have apparently disclosed that no known method of aging or flashing of a tungsten filament is successful in eliminating the ions of impurities.

A summary of the data is given in Table I to show the range of the measurements. The first column indicates the order in which sets of observations were made. After the observations at 2550°K were made, a nickel tab holding one end of the filament, parted. The filament was replaced, the tube assembled, baked out, and the observations were continued.

## Conclusion

This investigation shows conclusively that the number of ions with given initial velocity components from tungsten at high temperatures into a high vacuum, irrespective of their nature, are in accord with Maxwell's law.

The above results do not substantiate the statement made by Schottky regarding ions of high energy, nor do they support the hypothesis that ions are emitted as a result of an irreversible process.

## Acknowledgment

The author wishes to express his appreciation to Professor Lloyd P. Smith for suggesting this problem and for his constant help during the course of the work. Grateful acknowledgment is made to the Faculty of the Department of Physics for the facilities and apparatus provided. He wishes also to thank Mr. Banta for the construction of the glass apparatus.

# Discontinuities of Resistance Associated with the Barkhausen Effect

C. W. HEAPS, *The Rice Institute*

(Received January 2, 1934)

**A nickel wire, under bending stress, shows a large discontinuity of magnetization. The resistance of such a wire has been examined with a sensitive Kelvin double bridge and a jump of magnetoresistance of magnitude $dR/R=6.35\times10^{-5}$ has been found associated with the magnetization jump. The negative results of Steinberg and Miroschnischenko are explained as being due to insufficient sensitivity of their apparatus. It is suggested that the resistance jump is due to small rotations of the saturated magnetization of small elements of the material, these rotations being due to alterations of the Lorentz field by reversals of magnetization in neighboring elements.**

WHEN a ferromagnetic body is subjected to a magnetizing force which changes smoothly and continuously its intensity of magnetization may exhibit sudden jumps called Barkhausen discontinuities. The electrical resistance of the body will, in general, also vary when its magnetization changes, but up to the present no jumps of resistance have been found to occur when the Barkhausen discontinuities occur. From a study of the way in which magnetoresistance varies with magnetization W. Gerlach[1] concludes that the irreversible discontinuities of magnetism are without influence on the electrical resistance. Recently Steinberg and Miroschnischenko[2] have performed an experiment expressly designed to detect these resistance jumps. They report that in a nickel-iron alloy showing large discontinuities of magnetization no sudden changes of resistance could be detected.

The writer[3] recently advanced reasons for believing that these resistance jumps should exist but did not offer adequate experimental evidence in support of this view. This experimental evidence has now been secured.

[1] W. Gerlach, Ann. d. Physik **12**, 894 (1932).

[2] D. Steinberg and F. Miroschnischenko, Phys. Zeits. d. Sow. **3**, 602 (1933).

[3] C. W. Heaps, Phys. Rev. **43**, 763, 945 (1933). The desirability of an experiment of the type described in this paper was suggested by K. Sixtus, of the General Electric Company. The writer wishes to acknowledge here the helpful criticism received from Dr. Sixtus in connection with previous papers.

## EXPERIMENTAL METHOD

The specimen was a wire of commercial nickel 15 cm long and 0.0096 cm in diameter. The wire was annealed in a Bunsen flame, stretched beyond the elastic limit, bent into a circular coil of about 2.3 cm diameter, and then thrust into a fine, straight, capillary glass tube. Under these conditions nickel shows a single large magnetic discontinuity when the specimen is being demagnetized. A search coil around the tube was connected to an amplifier and loudspeaker for the detection of the discontinuity. The wire was now inserted in a solenoid and connected so as to form one arm of a sensitive Wheatstone bridge. When the solenoid current was brought smoothly and continuously to a certain value (by the use of a slider on a long straight resistance wire) a jump of magnetization was indicated by a single sharp noise in the loudspeaker. Simultaneously the galvanometer of the bridge was suddenly deflected several centimeters. The mean of a number of observations gave $3.2\times10^{-5}$ as the decrease of resistance per ohm associated with the magnetic discontinuity.

In view of the negative results of Steinberg and Miroschnischenko a more careful test seemed in order. With a Wheatstone bridge the Peltier effect at the junctions of the nickel wire causes temperature differences which introduce a thermoelectromotive force in the circuit. Since the thermoelectric power of nickel is affected by magnetization there seemed to be a possibility that jumps of thermoelectric power were being observed instead of jumps of resistance.

To obviate this uncertainty a special type of Kelvin double bridge was constructed as follows. Another nickel wire similar to the first was prepared but it was several cm longer. The ends of this wire projected out of the capillary tube and out of the solenoid. The ends of two copper wires were soldered to each end of a 15 cm segment in the center of the nickel wire. (This segment was held straight by a 15 cm capillary tube.) These copper wires led to the galvanometer circuit of the double bridge. Resistances of the entire bridge were adjusted so that the current flowing from the nickel wire into these copper leads was the same at both junctions. The resistance measured by the bridge is the resistance of the segment between the copper leads, and any change of thermoelectric power of nickel with respect to copper will not affect the measurement under these conditions.

The 15 cm segment of nickel had a resistance of 2.09 ohms. The bridge was balanced by adjusting shunts across this segment. The galvanometer was of the four-coil, astatic-needle type provided with a triple iron shield. The sensitivity of the bridge was such that a value of $dR/R$ as small as $4\times10^{-7}$ would produce a deflection of 1 mm. (Here $dR$= change in resistance $R$ of the nickel segment.) Actually, because of temperature changes the galvanometer was subject to a slow, steady drift of perhaps 3 or 4 cm per minute, so that the above sensitivity was not realized practically.

The solenoid was 15 cm long and had an internal diameter of 5.5 cm, so that its field was not very uniform. A current of 1 ampere produced a field of 105.5 oersteds at its center. The specimen was supported axially in the solenoid and was packed in cotton to secure thermal insulation.

With this apparatus the magnetic discontinuity was found to produce a galvanometer deflection of almost 200 mm. The mean of ten trials gave a value of $dR/R=6.35\times10^{-5}$, the separate values all lying between $6.07\times10^{-5}$ and $6.51\times10^{-5}$.

In Fig. 1 a part of the right half of a magnetoresistance hysteresis cycle is shown. The upper curve was obtained as follows. A field of 1000 oersteds, applied to saturate the nickel, was quickly reduced to a specified value and the bridge balanced. The field was then brought to zero and a new balance secured. The resistance change indicated by the two different bridge settings was plotted in Fig. 1 as $dR/R$ for the specified field. The lower branch of Fig. 1 was obtained as follows. The nickel was saturated by the field of 1000 oersteds, the field was made zero and the bridge balanced, a small reverse field of specified magnitude was applied and the bridge again balanced. The resistance change indicated by the two bridge settings was then plotted as $dR/R$ for the specified field.

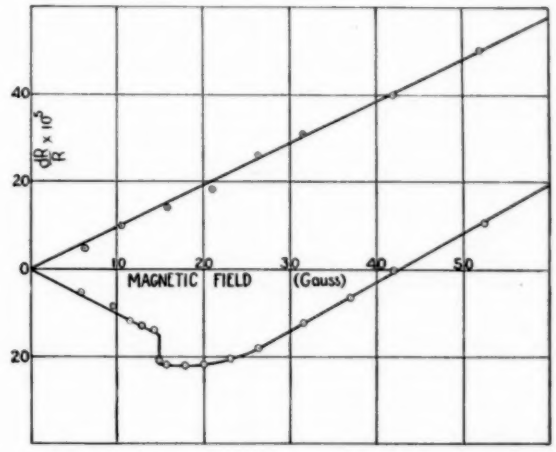


FIG. 1. Part of the right half of a magnetoresistance hysteresis loop of strained nickel. The abscissae should be multiplied by 10/14.7 if comparison is made with Fig. 2.

This method of procedure is necessary to secure accuracy when there is a temperature drift; the result is that Fig. 1 shows a value of $dR/R=0$ in zero magnetic field, although actually residual magnetism has left the wire with a higher resistance than it has when unmagnetized. The negative values of $dR/R$ are therefore not to be interpreted as a decrease of resistance produced by magnetization. The two branches of Fig. 1 join together, within the limits of experimental error, at about 600 oersteds.

Fig. 2 shows the magnetic hysteresis loop of this specimen of nickel, still in the strained condition inside the capillary tube. An astatic magnetometer similar to that of Bozorth[4] was used. The magnetizing solenoid was here 30 cm long so that the field was quite uniform. The magnetic discontinuity occurred in Fig. 2 at a

[4] R. M. Bozorth, J.O.S.A. and R.S.I. **10**, 591 (1925).

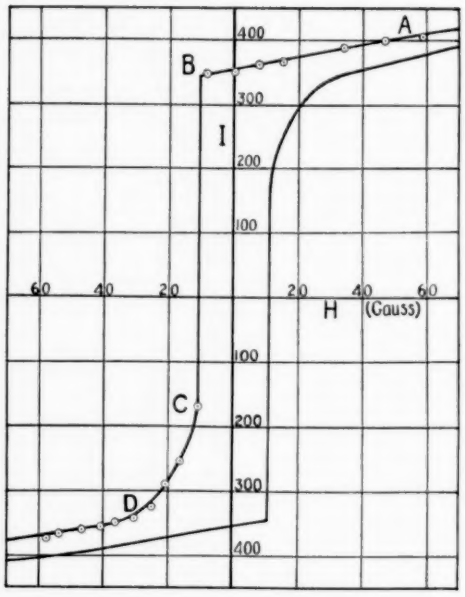


FIG. 2. Magnetic hysteresis loop of strained nickel. The right-hand branch is drawn in by symmetry.

demagnetizing field slightly greater than 10 oersteds, while in Fig. 1 the discontinuity of resistance is at 14.7 oersteds. The discrepancy is due to the fact that the solenoid of Fig. 1 did not give a very uniform field, and the field plotted is the maximum at the center. It was also observed that the demagnetizing field at the jump varied slightly with different trials, possibly because of temperature differences affecting the state of strain of the specimen.

## DISCUSSION

It appears that Steinberg and Miroschnischenko did not observe discontinuities of resistance because their apparatus was not sensitive enough. They state that a resistance change of $33\times10^{-6}$ ohm produced a galvanometer deflection of 1 mm. They do not give the resistance of their specimen, which was a wire 70 cm long, 0.038 cm in diameter, composed of 15 percent Ni and 85 percent Fe. Assuming the specific resistance to be $30\times10^{-6}$, as found by Yensen for this alloy, the resistance is calculated to be 1.8 ohms. The value of $dR/R$ producing a deflection of 1 mm is thus $18\times10^{-6}$. With a discontinuity of the size shown in Fig. 1, therefore, the apparatus of the Russian physicists would give a sudden galvanometer jump of about 3.5 mm. If the galvanometer were not quick in action, and if there were a slight temperature drift, such a small jump could hardly be detected.

There is also, of course, a possibility that in the matter of resistance jumps an iron-nickel alloy under tension does not behave like nickel under bending stress. From the standpoint of theory, however, it is not easy to see why the alloy should have no resistance jumps when the nickel exhibits them so decisively.

A comparison of Figs. 1 and 2 brings out certain points of interest. While the intensity of magnetization is decreasing along $AB$ in Fig. 2 a decrease of about 65 in $I$ produces a decrease of $58\times10^{-5}$ in $dR/R$. At the jump $BC$ a change in $I$ of 500 produces a $dR/R=6.3\times10^{-5}$. Where $I$ is increasing continuously from $C$ to $D$, changing by 155, the change in $dR/R$ is practically negligible, but as $I$ begins to show signs of saturation the $dR/R$ begins to show a more rapid rate of increase.

Apparently small resistance change is associated with steep parts of the hysteresis loop. It is precisely this characteristic which led Gerlach to suppose that magnetic discontinuities did not produce resistance discontinuities, inasmuch as magnetic discontinuities are largely confined to steep parts of the loop.

The current theories of magnetism assume a ferromagnetic body to consist of small elements magnetized to a saturation intensity $I_0$. The body as a whole is unmagnetized when the $I_0$ vectors of the small elements are oriented at random. An external field may magnetize the body by ($A$) sudden reversals of the directions of those $I_0$ vectors which oppose the external field, ($B$) rotation of the $I_0$ vectors into directions which more nearly agree with that of the applied field. Process $B$ is reversible, $A$ is irreversible. Discontinuities of magnetization are supposed to be due to process $A$.

It appears that process $A$ is not the only one involved in the magnetic discontinuities. From principles of symmetry process $A$ cannot be supposed to produce resistance changes. Neither could it produce magnetostriction changes. Since both resistance changes and length changes[5]

[5] C. W. Heaps and A. B. Bryan, Phys. Rev. **36**, 326 (1930).

appear in conjunction with magnetic discontinuities we must assume other processes than $A$ to be operative.

It seems probable that when the $I_0$ vector of one element reverses, the local magnetic field in which a certain specified neighboring element finds itself is changed. This field is the sum of the external field and the Lorentz field of neighboring doublets. The change of the Lorentz field due to sudden reversals of nearby doublets can cause a rotation of type $B$ in the specified element. This rotation, possibly through only a small angle, can cause a change of length and a change of resistance. (This conclusion follows from the fact that magnetostriction and magnetoresistance have quite different values depending upon whether they are measured along the direction of saturated intensity of magnetization or at right angles thereto.) According to this view the resistance jump of Fig. 1 is due to the summation over all elements of rotations of type $B$, these rotations being produced by sudden changes of the Lorentz fields of the elements. The sudden changes of the Lorentz fields are produced by reversals of type $A$ which occur in neighboring elements.

It appears that these rotations of type $B$ produced in this way are small, hence the magnetoresistance on the part of the hysteresis loop where discontinuities prevail—that is, on the steep parts—is small.[6]

A third type of change of $I_0$ has been suggested in which the vector suddenly swings through 90° in an unstrained cubic crystal. If the Barkhausen effect is due to this kind of process it could have magnetoresistance and magnetostriction associated with it inherently, and there would be no necessity of considering effects due to secondary rotations of neighboring elements. However, the small size of the resistance discontinuities would seem to be an objection to this theory.

---

[6] The Editor of the *Physical Review* has pointed out that the resistance jump will probably become smaller as the magnitude of the magnetic discontinuity increases. This conclusion appears to be true because complete reversal in all domains would reverse the Lorentz fields as well as the magnetization of each element, and hence no change of resistance would occur.

# Elastic Behavior and Elastic Constants of Zinc Single Crystals

ALVIN W. HANSON, *Physical Laboratory, University of Iowa*

(Received November 17, 1933)

The elastic constants are determined from bending and torsion experiments on single crystal rods. It is shown that for each crystal orientation there is a definitely limited region of proportionality between an initially increasing stress and the corresponding strain. The elastic region is a minimum (and very small) for crystals of 45° orientation. Elastic hysteresis occurs for bending but not for torsion, except for previously permanently strained crystals. There is no permanent set for stresses within the elastic limit. Two slightly different grades of very pure (99.99+ percent) zinc are studied. Their elastic behavior is in general alike, but the elastic constants differ appreciably. The constants found are: for Evanwall zinc, $S_{11}=8.08$; $S_{12}=1.57$; $S_{13}=-7.85$; $S_{33}=26.28$; $S_{44}=25.15$; for Horsehead Special zinc, $S_{11}=7.70$; $S_{12}=0.45$; $S_{13}=-6.39$; $S_{33}=27.66$; $S_{44}=24.40$, all times $10^{-13}$ cm²/dyne. The single crystal form possesses a definite and reproducible elastic behavior in contrast with the puzzling and variable results obtained for the polycrystalline and technically usable material.

## INTRODUCTION

THE elastic constants of the zinc crystal have been determined by Grüneisen and Goens,[1] Bridgman[2] and Goens.[3] Considering the different methods used and the probable differences in purity of the zinc, the general agreement in final values of the constants is surprisingly good. There are, however, sufficient discrepancies and scattering of individual results to justify a new determination. The present work is not confined simply to an accurate determination of the constants, but in addition a general study has been made of the elastic properties, including such matters as hysteresis, elastic limit, etc. The effect on the constants of very small amounts of impurity in the zinc is brought out by the use of two different brands of zinc both of the same high purity but differing somewhat in relative amounts of individual impurities present.

For the zinc crystal there are five elastic constants,[2,4] $S_{11}$, $S_{12}$, $S_{13}$, $S_{33}$, $S_{44}$. In terms of these it is possible to compute Young's modulus, $E$, and the rigidity modulus, $T$, of a crystal rod or bar of orientation,[5] $\varphi$ by the following relations:

$$1/E=S_{11}\sin^4\varphi+S_{33}\cos^4\varphi+(2S_{13}+S_{44})\sin^2\varphi\cos^2\varphi \quad (1)[4]$$

$$1/T=S_{44}+(S_{11}-S_{12}-\tfrac{1}{2}S_{44})\sin^2\varphi+2(S_{11}+S_{33}-2S_{13}-S_{44})\sin^2\varphi\cos^2\varphi. \quad (2)[6]$$

It would appear from these that if $E$ and $T$ (or $T$ alone) were measured for enough differently oriented specimens all constants could be obtained by the simultaneous solution of the equations resulting from substituting measured values in (1) and (2). There is one outstanding objection to this procedure: Except for some particular orientations the strain corresponding to a given stress is not always of the same type, i.e., a crystal beam to which a uniform bending moment (longitudinal stress) is applied, shows not only longitudinal strain but in addition an axial twist. If, thus, uniform bending is used to determine Young's modulus the usual formula for isotropic substances is only applicable in the absence of the effect just mentioned, and thus for crystals of particular orientations only. Similar remarks apply to the determination of the rigidity modulus by the usual torsion method.

[1] E. Grüneisen and E. Goens, Zeits. f. Physik **25–26**, 235 (1924).

[2] P. W. Bridgman, Proc. Am. Acad. Arts and Sci. **60**, 305 (1925).

[3] E. Goens, Ann. d. Physik **16**, 793 (1933).

[4] W. Voigt, *Lehrbuch der Kristallphysik*, p. 746.

[5] The angle between the hexagonal axis and the axis of the rod.

[6] W. Voigt, *Lehrbuch der Kristallphysik*, p. 747, Eq. (448).

This point has been discussed fully by Voigt[7] and Goens.[8] For hexagonal crystals of either 0° or 90° orientation this reciprocal bending-torsion effect is zero. Goens[8] has shown that it is also zero for zinc crystals of 70° orientation and nearly zero for all orientations between 70° and 90°. Moreover, more accurate values of the constants are obtained if, wherever possible, observations are made on specimens so oriented that each yields a single constant. Thus if $\varphi=0°$, $1/E=S_{33}$ and $1/T=S_{44}$. If $\varphi=90°$, $1/E=S_{11}$. Constants which cannot be determined singly, as just described, occur in combinations which will be discussed later.

As already inferred, two types of deformation were chosen, uniform bending, and longitudinal torsion, yielding Young's modulus, $E$, and the rigidity modulus, $T$, each of course, for the particular orientation of the single crystal specimen on which the determination is made.

## Material

The crystals were grown from two brands of zinc of very high purity (99.99+ percent), Evanwall[9] and Horsehead Special.[10] A detailed and semiquantitative spectral analysis was made with a quartz prism spectrograph (19 cm length spectrum; 5800–2500A) and the intermittent arc method of Gerlach and Riedl.[11] The impurity lines were brought out in larger numbers and with greater intensity by this method than by either the condensed spark or uninterrupted arc. For the Evanwall zinc analyses were made of a test or comparison sample of known chemical composition,[12] samples from the two lots from which crystals were made, and of some of the crystals themselves. The Horsehead Special zinc crystals were made from one lot, a single 50 lb. slab. Representative samples and crystals were analyzed. The analyses showed definitely that no detectable contamination was introduced during growth of the crystals and that the two lots of Evanwall were identical with the test sample. The two grades of zinc are compared in Table I in which are summarized the results of about 150 spectrograms, the numbers indicating the number of lines found. The comparative number of lines present or the relative intensity of a given line for a particular impurity gives some clue to the relative amount present in comparison with the test sample of Evanwall zinc the analysis of which is also included in Table I. The Horsehead Special zinc is definitely richer in iron and more nearly free from copper than the Evanwall.

Table I. *Comparison of two zinc samples.*

*f* indicates a faint line. *i* indicates that the line is intense. The chemical analysis of the Evanwall test sample shows: Fe 0.0004%, Cd 0.0008%, Pb 0.0047%, Cu 0.0002%, As, Co, Ni, Al, 0.0000%.

| | Ag | Cd | Cu | Fe | Pb |
|---|---|---|---|---|---|
| Horsehead Special | 0 | 4*f* | 1*f* | 32 | 6 |
| Evanwall test sample and lots 1 and 2 | 1 | 1 | 2*i* | 3*f* | 7 |

## Preparation of Crystals

The crystals were grown by a modified Kapitza[13] method. The specimens used for bending were rectangular (almost square) in cross section, being about 7 mm on a side, and 8 to 12 cm long. An asbestos board (Transite) with a groove of the correct shape served as a mold. It was smooth enough to permit the crystal to contract during cooling without strain. It has been found that if a crystal is not permitted to contract freely during cooling the basal planes present a warped appearance when cleaved. Under these circumstances also there is a great tendency to produce a multiple crystal or a new orientation altogether. The crystals used in the torsion experiments were cylindrical rods approximately 6 mm in diameter and 9 to 11 cm long. To prepare these, polycrystalline zinc rods were first cast in glass tubes and then removed from the tube and completely embedded in alundum cement. These rods were then placed in

[7] W. Voigt, *Lehrbuch der Kristallphysik*, p. 725.

[8] E. Goens, Ann. d. Physik **15**, 455 (1932) and **16**, 793 (1933).

[9] Evans Wallower Zinc Co.

[10] The New Jersey Zinc Co.

[11] W. Gerlach and E. Riedl, Phys. Zeits. **34**, 516 (1933).

[12] This sample and its chemical analysis were very kindly sent to Professor Tyndall by Mr. W. H. Bitner of the Evans Wallower Zinc Co., January, 1931.

[13] P. Kapitza, Proc. Roy. Soc. **A119**, 358 (1928). See also Soroos, Phys. Rev. **41**, 516 (1932).

the furnace and grown as before by fusing on a nucleus and cooling from the nucleus end. This method permitted growth with very little strain and produced crystals with uniform cross section. A few specimens were grown in glass tubes, but they were very much strained during growth as evidenced by slip bands on their surfaces and a pronounced warping of the basal plane.

## Apparatus

The bending apparatus is shown diagrammatically in Fig. 1. It is especially designed to compensate for any possible settling of the

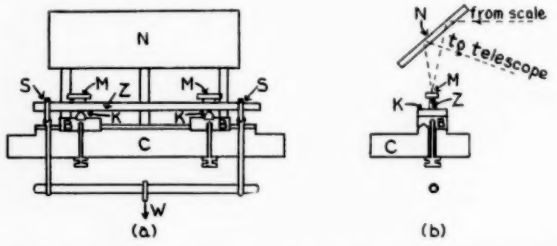


Fig. 1. Bending apparatus, vertical section; (a) parallel (b) perpendicular to length of crystal rod. *C*, cast iron base; *B*, adjustable brass blocks; *K*, knife edges; *S*, stirrups; *M*, small mirrors; *N*, large mirror; *Z*, crystal.

crystal on the knife edges or for any other motion of the crystal as a whole. This compensation is effected by use of two mirrors, $MM$, each of which forms an image of a distant scale. The images are viewed by two telescopes and the change in the difference in scale readings gives the change in the angle between mirrors for an applied load. A mercury reservoir applies the load at $W$. The load can thus be varied continuously without subjecting the crystal to the shock of sudden change in load. A careful calibration was made of the force produced by various levels of mercury in the reservoir.

The mirrors, $MM$, were at first mounted on the specimen by means of small balls of wax but this method caused spurious results due apparently to the plasticity of the wax. The scheme shown in the diagram was then adopted, the mirrors being mounted in a tripod setting. When placed on the surface of the crystal they are held in position by their own weight. This method of mounting has proved very satisfactory.

Torsion measurements were made on a specially constructed static torsion apparatus, which need not be described in detail as it involves no departure from the usual type. Very high grade ball bearings were used, however, in order to reduce to a minimum friction and "sticking"[14] when passing from increasing to decreasing load and *vice versa*. The loading was made continuous by a calibrated hanging chain arrangement. Square section end blocks of Wood's metal were cast on the crystals in order to fasten them in the torsion apparatus. Light mirrors were fastened to the crystals with weak spring slips and observations were made with two telescopes and a scale as in the bending experiments. Since the load for both bending and torsion was increased slowly and continuously and since at least a minute more was required to take the readings it is assumed that the results are isothermal.

## Results

Twelve Evanwall and four Horsehead Special crystals were used in the bending experiments. A run with increasing load and immediately following decreasing load was taken on each crystal soon after growth. The crystals were handled with extreme care before and during these runs. Crystals of the same orientation[15] of both sorts of zinc behaved alike. Typical stress-strain diagrams of three crystals of different orientation are shown in Fig. 2.[16] The relation between stress and strain is strictly linear on each ascending branch.[17] From its slope, $\theta/Q$, the Young's modulus is determined by the usual relation,[18] $E=12Q/BD^3\theta$, in which $Q$ is the

[14] See curves of Fig. 3 which represent actually observed results, that is, no correction or shifting of the curves has been made to allow for friction or "sticking."

[15] The actual orientations of the crystals may be seen from the plot of Fig. 4, curves (a) and (b). At 90° there are four Evanwall crystals, two pairs of points being identical, and two nearly coincident Horsehead Special crystals.

[16] For curve (b) the initial strain, corresponding to zero stress, is zero. The curve has been raised for convenience in plotting. The same observation applies to curves of other figures in which groups of similar curves are plotted together.

[17] These curves cover about 90 percent of the region in which linearity holds. The descending branch is discussed later.

[18] Strictly applicable only to crystals of nearly 0° and 70°–90°.

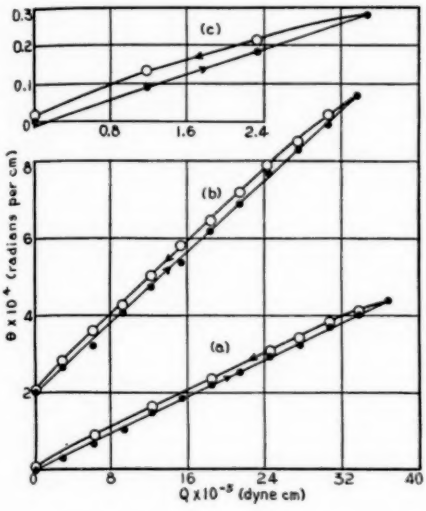


FIG. 2.

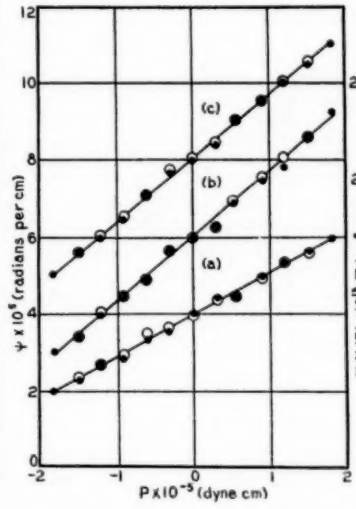


FIG. 3.

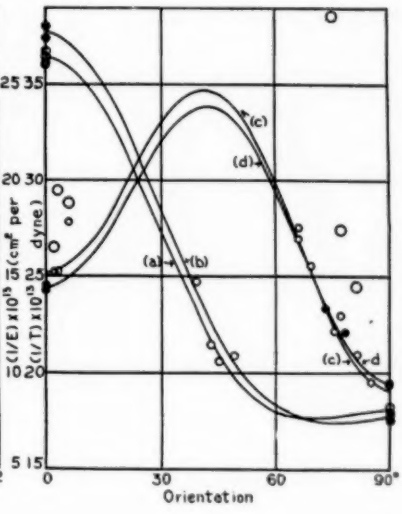


FIG. 4.

FIG. 2. Curvature $\theta$ of uniformly bent crystals as dependent on bending moment $Q$ for initially strain free crystals. Orientations and $BD^3$ are: (a) 90°, 0.0805 cm⁴; (b) 0°, 0.144 cm⁴; (c) 49°, 0.161 cm⁴.

FIG. 3. Angle of twist per unit length $\psi$ as dependent on applied axial torque, for initially unstrained or annealed crystals. Orientations and radii are: (a) 90°, 0.327 cm; (b) 0°, 0.306 cm; (c) 75°, 0.302 cm.

FIG. 4. Reciprocal of Young's modulus, curves (a) and (b), and reciprocal of rigidity modulus, curves (c) and (d) as a function of the orientation. Curves (a) and (c), with the small open circles representing the experimental observations for individual crystals, are for Evanwall zinc. Similarly curves (b) and (d), with the closed circles, represent the Horsehead Special zinc. The large open circles represent values of the reciprocal of the rigidity modulus for crystals in the strained condition.

bending moment, $\theta$, is the curvature of the beam, and $B$ and $D$ are the breadth and depth, respectively.

Torsion measurements were made on ten Evanwall and six Horsehead Special crystals. Runs were taken in this case from zero torque to a maximum[19] in one direction, to an equal reverse maximum, and back to zero. Typical curves are shown in Fig. 3. Proportionality of stress and strain is again definitely indicated. Moreover there is no observable separation depending on direction of loading. From the slopes, $\psi/P$, of these curves the rigidity modulus is determined as usual from $T=2P/r^4\psi\pi$,[18] in which $P$ is the torque, $r$ the radius of the rod, and $\psi$ the twist per unit length.

The elastic constants are obtained, in a fashion to be described below, from the value of $E$ or $T$ for each crystal found from curves like those of Fig. 2 (ascending branches) and Fig. 3. In Table II are collected the values of the constants for the two brands of zinc and the values from previous investigations. The cubic compressibility, $K$, and the linear compressibilities parallel, $K_{||}$, and perpendicular, $K_\perp$, to the hexagonal axis are also included. They are computed from the constants in the usual fashion. $K=2K_\perp+K_{||}$.

TABLE II. *The elastic constants and compressibilities of single crystal zinc in cm² dyne⁻¹ × 10⁻¹³ at room temperature.*

| | Grüneisen and Goens | Bridgman | Goens | The present investigation: Evanwall | The present investigation: Horsehead Special |
|---|---|---|---|---|---|
| $S_{11}$ | 8.0 | 8.23 | 8.4 | 8.08 | 7.70 |
| $S_{33}$ | 28.2 | 26.38 | 28.7 | 26.28 | 27.66 |
| $S_{44}$ | 25.0 | 25.0 | 26.4 | 25.15 | 24.40 |
| $S_{12}$ | −0.5 | 0.34 | 1.1 | 1.57 | 0.45 |
| $S_{13}$ | −6.05 | −6.64 | −7.75 | −7.85 | −6.39 |
| $K_{||}$ | | 13.10 | 13.20 | 10.58 | 14.88 |
| $K_\perp$ | | 1.93 | 1.75 | 1.80 | 1.76 |
| $K$ | | 16.96 | 16.70 | 14.18 | 18.40 |

The $1/T$ and $1/E$ curves of Fig. 4 are computed from the relations (1) and (2) and the values of constants from Table II. These plots bring out the general elastic behavior of the two zincs as a function of orientation. The plotted points show the actually measured values of all the individual crystals. The points indicated by

[19] At about 80 percent of the elastic limit.

the larger circles in Fig. 4 are values[20] of $1/T$ for crystals measured in a strained condition. The small circles at the same orientation as the larger are the values obtained after these crystals have been annealed for nine hours at 380°C. In every case the elasticity is raised (values of $1/T$ reduced) by the anneal. In two cases ($\varphi=6°$ and 77°) the strain does not seem to have been completely removed. Moreover the 6° crystal showed some torsional hysteresis (see next section) after annealing.

Since there are various ways of deriving values of the constants from the experimental data it may be well to make some specific statements as to the methods adopted. For the Evanwall and Horsehead Special zinc both 0° and 90° orientations were used in bending, and $S_{11}$ and $S_{33}$ are determined directly from these orientations without reference to any others. For the Horsehead Special zinc two 0° crystals were available for torsion, yielding $S_{44}$ directly. For the Evanwall zinc there were two crystals having orientations of 2° and 3°. For them $S_{44}$ was obtained by substitution in Eq. (2), a preliminary set of constants[21] being used in the numerically small terms containing $\sin^2\varphi$, giving practically a direct value of $S_{44}$. For the Horsehead Special zinc $S_{12}$ is obtained from torsion of two 90° crystals, since substitution of $\varphi=90°$ in Eq. (2) gives $1/T=S_{11}-S_{12}+\frac{1}{2}S_{44}$ in which two constants are already known. For the Evanwall zinc $S_{12}$ is obtained from one 85° crystal in similar fashion.[22] With $S_{12}$ known, $S_{13}$[23] is determined from relation (2). For the Evanwall zinc the data of four crystals are considered, $\varphi=66°$ (two crystals), 69° and 75°. Data for two Horsehead Special crystals, $\varphi=73°$ and 78°, yield $S_{13}$ for that material.

From a study of the elastic constants given in Table II it appears certain that the elasticity of zinc is very sensitive to small variations in amount and kinds of impurities. The difference in the constants for Evanwall and Horsehead Special zinc is too great to be accounted for by experimental error or difference in treatment of the two brands of zinc as the crystals were grown and measured under like conditions. It is to be noted that the constants of Evanwall zinc resemble more closely those given by Goens while the Horsehead Special zinc constants resemble those given by Bridgman. This sort of resemblance renders it probable that the difference between the results of Bridgman and Goens is genuine and may be attributed to differences in materials. In the values of the compressibilities given in Table II there is good agreement for $K_\perp$ but $K_{||}$ for the Evanwall zinc appears exceptionally low. In order, however to get a value of $K_{||}$ about equal to that of the other zincs, $S_{33}$ would have to be 10 percent greater or $|S_{13}|$ 15 percent less. A variation of this magnitude in either of the two constants is definitely inconsistent with the experimental results. If there is to be any variation the results would rather indicate a greater value of $|S_{13}|$.[24] The low cubic compressibility of Evanwall zinc is due entirely to the low value of $K_{||}$. The data available for independent experimental checks on the cubic compressibility are for polycrystalline zinc. Bridgman[25] gives such values ranging from $8.5\times10^{-13}$ to $24\times10^{-13}$; Adams, Williamson and Johnston[26] give $17.3\times10^{-13}$. The latter value is in fairly good agreement with all except the Evanwall zinc, but in view of the large scattering and the peculiar hysteresis effects, etc., found by Bridgman, it seems necessary to suggest that perhaps this good agreement is largely fortuitous and that on the contrary one should not expect

[20] These are figured from the general slope of the hysteresis loop; see next paragraph.

[21] Previously determined by the writer.

[22] Actually, since the crystal is not exactly 90°, a method of successive approximation was employed by using relation (2), and successively closer values of $S_{13}$.

[23] For the sake of comparison one may neglect the reciprocal torsion-bending effect previously discussed and determine the constant $S_{13}$ from the bending of four Evanwall crystals of nearly 45° orientation. Use of Eq. (1) yields; $1/E=\frac{1}{4}(S_{11}+S_{33}+2S_{13}+S_{44})$ and the numerical values; $S_{13}=-3.75$, $-8.52$, $-8.52$ and $-4.34$ averaging $-6.30\times10^{-13}$ cm²/dyne.

[24] Admittedly $S_{13}$ is not known with as great accuracy as if it had been determined independently as was $S_{33}$ and it is therefore the one under suspicion. The results for strained crystals, however lead to smaller values of $|S_{13}|$ and therefore the largest values obtained should be given most weight.

[25] P. W. Bridgman, Proc. Am. Acad. Arts and Sci. **58**, 166 (1923).

[26] Adams, Williamson and Johnston, J. Am. Chem. Soc. **41**, 12 (1919).

good agreement of computed values with values determined from experiments on polycrystalline samples, especially in view of the possibilities of mutual constraint[27] of the individual grains in a material with such large elastic anisotropy as zinc. There seems to be no great objection to supposing that different brands of zinc are likely to show as great or greater variation in the three compressibilities than that found in the Evanwall and the Horsehead Special.

### Hysteresis

In the torsion experiments on unstrained crystals no detectable hysteresis appears (see Fig. 3). Strained crystals under torsion show no region of proportionality between stress and strain and give wide hysteresis loops. Curve (a) of Fig. 5 is for a strained[28] crystal while curve (b) shows the results obtained on the same crystal after annealing.

In bending, a small amount of hysteresis is always present. Typical cases are shown in Fig. 2. The decreasing load curve is convex upward and does not coincide with the increasing load curve, even when the latter is the first run taken on a crystal after growth. An anneal does not remove this hysteresis and it is believed to be typical of the unstrained material. There is no detectable permanent set and the cycle can be repeated indefinitely. The hysteresis is of the type usually called elastic. It has been found to occur, for instance, in the bending of rocksalt crystals[29] but only after the material has suffered an initial permanent deformation. It is remarkable that hysteresis occurs for bending (longitudinal stress and strain) and not for torsion (shearing stress and strain).

The presence of hysteresis is exceedingly interesting. Such theory as there is for metal crystals seems to lead to the expectation of no hysteresis in ideally perfect crystals. Whether the hysteresis is to be ascribed to the very minute amount of impurities, following some such theory as Prandtl's, or whether it is due to a lack of perfection in the real crystals, such as the existence of the secondary structure of Zwicky, cannot be decided in the light of the foregoing experiments.

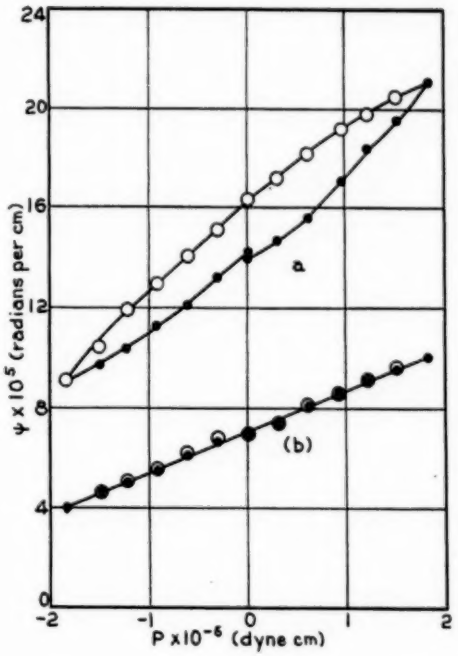


Fig. 5. Torsional hysteresis in a strained crystal and effect of annealing. (a) strained crystal; (b) same crystal after annealing.

### Strain Beyond the Elastic Limit and Creep

If the curves of Fig. 2 are extended the results pictured in Fig. 6 are obtained. This is for a crystal of 90° orientation. With the elastic limit defined as the rather definite limit of proportionality, the figure shows quite plainly that a crystal strained well beyond this limit will show permanent set when the load is reduced to zero, but will on a subsequent strain, which is kept below this limit, show the same type of elastic hysteresis (small loop in the figure) as before. The value of Young's modulus for the second increasing load is very slightly lower (about 1 percent).

Creep is also shown in the figure, as a pause of one hour intervened between the two points at $Q=51\times10^5$ dyne cm. This creep was watched. About 60 percent occurred in the first ten

[27] Bridgman has hypothecated such an effect from observations on a double crystal.

[28] This crystal was grown in a glass tube and was strained both during growth and on removal from the tube.

[29] Polyani and Sachs, Zeits. f. Physik **33**, 692 (1925).

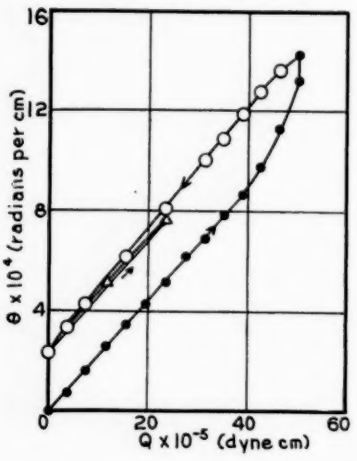


FIG. 6. Plastic deformation and creep.

minutes but it had not quite ceased at the end of the hour. It was also definitely observed, both for torsion and bending, that, while in Fig. 6 the elastic limit has been exceeded by about 30 percent, the same phenomena pictured there occur also if the elastic limit is exceeded by something less than 10 percent. Thus if the yield point and the limit of obedience to Hooke's law are not coincident they are very close together.[30]

## ELASTIC LIMIT

In the case of bending the observed quantity is the curvature ($\theta$) of the beam at which plastic deformation starts. Since this presumably occurs first along fibers at the greatest distance above and below the median plane the limiting longitudinal strain is given by $\Delta L/L=\frac{1}{2}D\theta$. For four 90° Evanwall crystals the average value is $\Delta L/L=0.93\times10^{-4}$, individual values ranging from 0.8 to $1.1\times10^{-4}$. The elastic limit[31] for 0° crystals in bending is at least twice as high. The limit for 45° (or nearly so) orientations is exceedingly low. One Evanwall crystal ($\varphi=49°$) had a limiting value, $\Delta L/L=1.8\times10^{-6}$.

From $E$ and $\Delta L/L$ for each case it is possible to compute the corresponding longitudinal stress at the limit of elasticity. These are shown in Table III with values from Schmid[32] and Rosbaud and Schmid.[33] The agreement for the high and the low orientations is fairly good. For the intermediate orientations the writer's much lower elastic limit is no doubt due to a greater purity[34] of material. The low elastic limit of crystals near 45° orientation also points to an exceedingly great ease of slipping of the basal planes over each other, provided the component of stress in the basal plane has a large component in the direction of a single digonal axis of the first kind, this being the direction of easiest "glide." Schmid, for instance, for a group of crystals with orientations between 75° and 32° finds the component of stress in the "glide" direction to be almost constant with a mean value of 18.3 $\times10^6$ dynes/cm², whereas the corresponding value for the writer ($\varphi=49°$) must be about[35] $0.9\times10^6$ dynes/cm².

TABLE III.

| Orientation | Limiting stress $\times10^6$ dynes/cm² |
|---|---|
| 83° | 73 R. and S. |
| 90° | 115 A.W.H. |
| 75° | 97 S. |
| 49° | 1.8 A.W.H. |
| 56° | 30 S. |
| 46° | 17 R. and S. |
| 0° | 71 A.W.H. |
| 13° | 45 R. and S. |

For torsion the elastic limits of two Evanwall crystals, 2° and 85°, are: $\psi=5.21$ and $6.1\times10^{-5}$ radians/cm. This gives for the outer layer, in which the shear is greatest, shearing strains, $1.705\times10^{-5}$ and $1.86\times10^{-5}$, respectively. For the 2° crystal the corresponding shearing stress is $6.77\times10^6$ dynes/cm². Since this stress lies in

[30] For this reason the writer has considered (see below) the "Streckgrenze" of Rosbaud and Schmid as coincident with the elastic limit.

[31] The writer has not determined this accurately on account of the danger of breaking a 0° crystal when strained beyond the elastic limit.

[32] E. Schmid, Zeits. f. Physik **40**, 54 (1926).

[33] P. Rosbaud and E. Schmid, Zeits. f. Physik **32**, 197 (1925).

[34] Spectral analyses of samples of Kahlbaum zinc always show distinctly more cadmium than found in Evanwall zinc. The presence of cadmium has been shown by Rosbaud and Schmid (reference 33) to increase the elastic limit.

[35] The positions of the digonal axes were not determined for the writer's crystals but one must lie within 30° of the projected stress component on the basal plane. The value quoted above might therefore be multiplied by some value between 1 and 0.866.

the basal plane it may seem remarkable that it is so much higher than the corresponding maximum shearing stress in the basal plane observed in the bending of the 49° crystal. It must be observed however that this stress varies in direction around the circumference of the cross section and does not, as in the case of bending, coincide with a *single* digonal axis of the first kind. There is therefore no tendency for glide in a single direction. For the 85° crystal the maximum stress (on the circumference of the cross section) lies in the basal plane only at the ends of a certain diameter while at the ends of the perpendicular diameter there is no component of shearing stress in the basal plane. From the known maximum strain it is possible to compute the maximum stress in the basal plane. It is given by: $1.85\times10^{-5}/S_{44}$ or $7.4\times10^{6}$ dynes/cm². The corresponding stress (in a plane perpendicular to the basal plane) at the ends of the second diameter is given by: $1.85\times10^{-5}/2(S_{11}-S_{12})$, or $14.3\times10^{6}$ dynes/cm².

It is conceivable that for crystals of both 90° and 0° permanent slip first occurs somehow along the basal plane but it is not related to a *single* glide direction and the elastic limit for both 90° and 0° should therefore be and are about the same, and are high relative to the elastic limit for the bending of a 45° crystal; nor should the torsion of intermediate orientations show an abnormally low elastic limit.

## Polycrystalline Zinc

The behavior of a cast polycrystalline bar subjected to bending is shown in Fig. 7. The same results are obtained whether the bar is measured as cast or with subsequent annealing (nine hours at 380°C). It will be noticed that there is no region of proportionality for an initial increasing load. A cyclic state is however established (small loop) on a second loading. The hysteresis is greater and of slightly different type from that shown by the single crystals. From the slope of the practically straight line drawn through the four solid circles on the small loop the reciprocal modulus is computed to

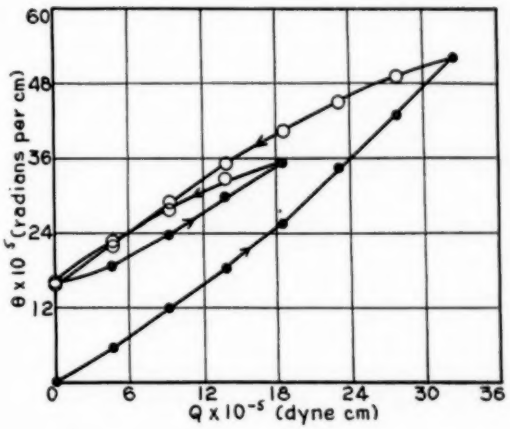


Fig. 7. Bending of a polycrystalline rod.

be: $1/E=10.60\times10^{-13}$ cm²/dyne. An exactly similar effect for polycrystalline zinc bars subjected to bending has been observed by Dalby.[36] In view of the elastic limit to be expected for crystals of orientations in the neighborhood of 45° it is not surprising that polycrystalline zinc shows practically no region of proportionality between stress and strain and explains why zinc, particularly under tensile test, is said in the literature[37] to be "imperfectly elastic" and that it is "doubtful if the elastic limit has any special physical significance." The above experiments afford a ready explanation of these facts since in any cast polycrystalline specimen there would be many crystallites of such orientation to the applied stress that their elastic limit would be exceeded under a very low value of the stress, or might even be exceeded during the uneven contraction of individual grains which occurs during the cooling of a casting. Their plastic extention for higher stresses would give a curve of the type of Fig. 7.

In conclusion, the author wishes to express his sincere thanks to Dr. E. P. T. Tyndall, for suggesting this problem and for his many helpful suggestions and criticisms during the course of this research.

[36] Dalby, Phil. Trans. Roy. Soc. London **A221**, 117 (1920).

[37] Moore, quoted in B.S. circular No. 395, p. 89.

# The Thermodynamic Properties of Helium Gas

J. R. ROEBUCK AND H. OSTERBERG, *Physical Laboratory, University of Wisconsin*

(Received May 29, 1933)

The Joule-Thomson coefficients of the preceding article and the *pv* data of Holborn and Otto are here used to calculate the most important thermodynamic properties of helium. The *variation of the specific heat with pressure* is small. The computed values of the *specific volumes* compare excellently with those from the data of Holborn and Otto. Simple relationships are shown to exist between *the coefficient of free expansion* $\eta$ *and the intrinsic energy variation* $\lambda$. Convenient equations are derived for computing these coefficients. $\eta$ is independent of the pressure and $\lambda$ is proportional to the square of the pressure except at the lowest temperatures. Both $\eta$ and $\lambda$ are zero at about $-70$°C, are positive below this temperature and are negative above. Their numerical value above $-70$°C is everywhere small. The pressure and temperature behavior of $\eta$ and $\lambda$ is explained by a kinetic theory taking into account the change in the total potential energy stored by collision between the helium atoms when the pressure is altered. The law of force between two helium atoms, consistent with this theory, is of the type giving rise to the same mutual potential energy of two helium atoms as deduced from considerations of the quantum theory. It is extremely doubtful that the trend of $\eta$ at high temperature leads ultimately to the perfect gas state.

THE isenthalpic curves for helium between $-190$ and $+300$°C over the pressure range 1 to 200 atm. have been given in a preceding article.[1] These experimental curves are straight lines over this temperature-pressure range except at the lowest temperatures. The slope of these lines, $\mu$, called the porous plug coefficient, has also been given with some discussion of its significance.

As in the similar work with air,[2, 3] this coefficient may be combined with specific heat and *pv* data to yield, often with high precision, a variety of thermodynamic properties. Among these the free-expansion coefficient, $\eta \equiv (dT/dp)_u$, previously quite unknown, is of great interest as giving direct experimental information about the dependence of the law of force between molecules upon both pressure and temperature. This is of immediate application in the atomic structure studies. The variation of intrinsic energy with volume at constant temperature, $\lambda \equiv (du/dv)_T$, raises some interesting questions by its negative sign.

## SPECIFIC HEAT $C_p$

The specific heat of helium has been measured by several workers. The best determinations are those by Scheel and Heuse.[4] They give

| $t$ | $-180$°C | 18°C |
|---|---|---|
| $C_p$ | 1.237 | 1.251 |

in calories per gram degree. These are the only available data on the variation of $C_p$ with temperature.

The meagerness of this knowledge of $C_p$ as a function of temperature prevents the spreading of the values over the pressure range as in the air work.[2] The most that can be done is to tabulate a factor which may be used to spread $C_p$ over the pressure range when it becomes known over a temperature range.

Thus in Fig. 1, the isenthalps $h_1$ and $h_2$ are straight lines of slope $\mu_1$ and $\mu_2$. One can therefore

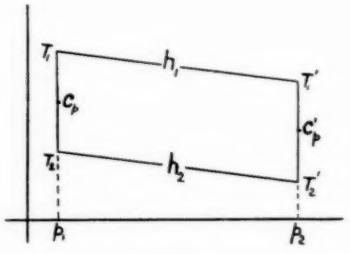


FIG. 1.

[1] Roebuck and Osterberg, Phys. Rev. **43**, 60 (1933).
[2] Roebuck, Proc. Am. Acad. **60**, 537 (1925).
[3] Roebuck, Proc. Am. Acad. **64**, 287 (1930).
[4] Scheel and Heuse, Ann. d. Physik [4] **37**, 79 (1912).

write

$$T_1 = T_1' + \mu_1(p_1 - p_2),$$
$$T_2 = T_2' + \mu_2(p_1 - p_2)$$

or

$$T_1 - T_2 = (T_1' - T_2') + (\mu_1 - \mu_2)(p_1 - p_2).$$

If $C_p$ and $C_p'$ are the average specific heats over the range indicated, then

$$\frac{C_p}{C_p'} = \frac{T_1' - T_2'}{T_1 - T_2} = 1 - \frac{\mu_1 - \mu_2}{T_1 - T_2}(p_1 - p_2)$$
$$= 1 + M(p_2 - p_1), \quad (1)$$

where $C_p'$ is the specific heat at the higher pressure. $M$ is a function of the temperature but not of the pressure. From the data of the previous article,[1] $M$ has been calculated and is given in Table I.

TABLE I. *Values of M.*

| $t$°C | $M\times10^5$ (atm.)$^{-1}$ | $t$°C | $M\times10^5$ (atm.)$^{-1}$ | $t$°C | $M\times10^5$ (atm.)$^{-1}$ |
|---|---|---|---|---|---|
| 275 | −6.2 | 125 | +1.2 | − 25 | 3.0 |
| 225 | −2.4 | 75 | 1.6 | − 75 | 4.2 |
| 175 | −0.6 | 25 | 2.2 | −125 | 13.2 |

This means, for example, that the difference between the $C_p$ at 1 and at 200 atm. at 275°C is about 1 percent. This difference in $C_p$ decreases to zero at 160°C and to −1 percent at −100°C. The following calculations cover the range 1 to 40 atm. and −50 to 150°C. The pressure variation of $C_p$ in this range is less than 0.1 percent.

The temperature range variation as measured by Scheel and Heuse[4] is 1.2 percent between 18 and −180°C. This variation, although it may be proportionately less between −50 and 150°C, handicaps seriously much of the following calculations and introduces uncertainty into some of the conclusions.

## Coefficient of Volume Expansion, $\alpha_p$

The equation[3]

$$\alpha_p \equiv (1/v)(dv/dT)_p = (1/T)[\mu C_p/v + 1]$$

was used to compute $\alpha_p$. $C_p$ was taken as constant. (See Table II.)

At the low pressure end of the range $\mu C_p/v$ is between 0.0009 and 0.0005 and if $\mu$, $C_p$, and $v$ are each known to 1 percent, $\alpha_p$ is relatively correct to one part in $10^5$. At the high pressure end of the range $\mu C_p/v$ lies between 0.025 and 0.013 so that here $\alpha_p$ is relatively correct to about a part in $10^4$. If only relative values are desired, these figures are probably better than any directly determined values. They are also excellent in the absolute sense, since this absolute value depends finally on the average coefficient 0–100°C which is undoubtedly the most carefully measured of any volume-temperature coefficient of helium.

TABLE II. $\alpha_p\times10^3$ *in* °$C^{-1}$.

| $p(m)$ | $p$(atm.) | −50°C | 0°C | 50°C | 100°C | 200°C |
|---|---|---|---|---|---|---|
| 1 | 1.31579 | 4.47738 | 3.65834 | 3.09260 | 2.67842 | 2.11256 |
| 5 | 6.57895 | 4.46183 | 3.64777 | 3.08485 | 2.67254 | 2.10887 |
| 10 | 13.1579 | 4.44253 | 3.63464 | 3.07521 | 2.66522 | 2.10427 |
| 20 | 26.3158 | 4.40448 | 3.60865 | 3.05612 | 2.65069 | 2.09511 |
| 30 | 39.4737 | 4.36714 | 3.58302 | 3.03723 | 2.63630 | 2.08602 |

## Specific Volume

In Fig. 7 of the earlier paper[1] that part of the curve between −50 and +150°C is almost a straight line, so that

$$\mu = \mu_0 + a(T - T_0)$$

where $a = -2.12\times10^{-5}$ atm.$^{-1}$; $\mu_0 = -5.98\times10^{-2}$ °C/atm.; $T_0 = 273.15$°K. The fundamental equation for the porous plug effect,

$$\mu C_p = T(dv/dT)_p - v, \qquad \text{(Eq. (2), p. 296)}^4$$

may be written

$$\frac{\mu C_p}{T^2} = \left(\frac{d(v/T)}{dT}\right)_p = \frac{C_p}{T^2}[\mu_0 + a(T - T_0)]$$

where $T$ falls between $-50$ and 150°C. Upon integrating,

$$\frac{v}{T}-\frac{v_0}{T_0}=C_p(\mu_0-aT_0)\left(\frac{1}{T_0}-\frac{1}{T}\right)+aC_p\log_e\frac{T}{T_0}\equiv E, \quad (2)$$

which will hold for any one constant pressure.

Since $v/T$ varies slowly along an isopiestic, $E$ is a small correction term. This equation has been used to calculate $v$ over the temperature range at each of a set of pressures from the above values of $a$, $\mu_0$, $T_0$ and values of $v_0/T_0$ properly chosen from the data of Holborn and Otto.[5] In this calculation $C_p$ was obtained from a linear extrapolation of the values of $C_p$ given by Scheel and Heuse.[4] The values of $v$ are given in Table III, where they are paired with values taken from Holborn and Otto's work. The uncertainty of 10–20 percent in the slope $a$ is the major source of error in these calculations. But the error introduced in the value of $E$ by this uncertainty is less than 3 percent. Since the error in the selected values of $C_p$ should be less than 1 percent, an error of 4 percent in $E$ in the temperature range $-50$ to 150°C is an overestimate. Values for $v$ at 200°C are also given in Table III. The error in $E$ at this temperature is less than one percent greater than in the values of $E$ for the range $-50$ to 150°C. The relative value of $E$ and $v_0/T_0$ for the various pressures in Table III is such that the above errors in $E$ introduce uncertainty of 2 in the sixth significant figure of the 1 meter row, the fifth of the 10 meter row, and the fourth of the 20, 30, and 40 meter rows. Since the errors estimated above are the maximum, this method of calculation is an excellent one for obtaining the temperature variation of the specific volume at constant pressure, and may be used to give more reliable values for this temperature variation than the directly measured values.

TABLE III. *Specific volume, v, in liters/gram. Holborn and Otto's data in italics.*

| $p$(m) | −50°C | 0°C | 50°C | 100°C | 200°C |
|---|---|---|---|---|---|
| 1 | 3.48045 | 4.25962 | 5.03875 | 5.81789 | 7.37612 |
| | *3.48063* | | *5.03871* | *5.81780* | *7.37580* |
| | −18 | | +4 | +9 | +32 |
| 10 | 0.350707 | 0.428604 | 0.506483 | 0.584360 | 0.740078 |
| | *0.350755* | | *0.506512* | *0.584378* | *0.740067* |
| | −48 | | −29 | −18 | +11 |
| 20 | 0.176851 | 0.215792 | 0.254719 | 0.293638 | 0.371445 |
| | *0.176879* | | *0.254725* | *0.293616* | *0.371418* |
| | −28 | | −6 | +22 | +27 |
| 30 | 0.118888 | 0.144842 | 0.170782 | 0.196714 | 0.248546 |
| | *0.118924* | | *0.170797* | *0.196710* | *0.248534* |
| | −36 | | −15 | +4 | +12 |
| 40 | 0.0899141 | 0.109376 | 0.128823 | 0.148264 | 0.187112 |
| | *0.0899503* | | *0.128821* | *0.148256* | *0.187091* |
| | −36.2 | | +2 | +8 | +21 |

A comparison of the calculated values of $v$ with those taken directly from the tables of experimental data of Holborn and Otto[5] shows excellent agreement. The slight deviations indicate no systematic error in the pressure variation and possibly a small systematic error in the temperature variation. These deviations are in most cases larger than our estimated maximum error and should therefore be interpreted as error in their data.

COEFFICIENT OF FREE EXPANSION, $\eta\equiv(dT/dp)_u$

For the first calculation of $\eta$ the equation[3]

$$\eta[C_p-(d(pv)/dT)_p]=\mu C_p+(d(pv)/dp)_T$$

was used. $C_p$ is again assumed constant as 1.251 cal./g °C. Since $(d(pv)/dT)_p=(pv)\cdot\alpha_p$, this was readily obtained from Holborn and Otto's data[5] and $\alpha_p$ from Table II. The data for $(d(pv)/dT)_p$ show a maximum variation over this range of temperature and pressure of only 0.7 percent. They are effectively constant over the pressure range. The term, $(d(pv)/dp)_T$, comes directly from Holborn and Otto's data under suitable modification of the units. The data show that this term varies only slightly over this temperature range and almost imperceptibly over the pressure range. $\mu$ and $C_p$ are both independent of the pressure. Hence $\eta$ is nearly independent of the pressure but varies with the temperature. The values of $\eta$ so obtained are listed in Table IV.

TABLE IV. $\eta[=(dT/dp)_u]$ *in °C/atm.*

| $t$°C | −50 | 0 | 50 | 100 | 200 |
|---|---|---|---|---|---|
| $-\eta\times10^3$ | 1.71 | 3.92 | 7.30 | 11.3 | 14.3 |

It will be observed that in the temperature range of Table IV, $\eta$ is negative, is very small, is

[5] Holborn and Otto, Zeits. f. Physik **30**, 320 (1924).

TABLE V. $\gamma$ *in atm.*$^{-1}$.

| $p(m)$ | −50°C | 0°C | 50°C | 100°C | 200°C | $p^{-1}$(atm.) |
|---|---|---|---|---|---|---|
| 1 | 0.759345 | 0.759471 | 0.759558 | 0.759629 | 0.759724 | 0.76 |
| 5 | .151352 | .151472 | .151545 | .151628 | .151712 | .152 |
| 10 | .0753545 | .0754743 | .0755589 | .0756292 | .0757135 | .076 |
| 20 | .0373604 | .0374779 | .0375616 | .0376308 | .0377145 | .038 |
| 30 | .0246996 | .0248149 | .0248975 | .0249660 | .0250489 | .02533 |

independent of the pressure and increases numerically with rising temperature. The negative sign was entirely unexpected, since it means that helium becomes warmer on free expansion, and led to a careful check on these calculations. The possibility of a gas warming on free expansion is excluded in current texts on heat and kinetic theory which in the light of these data require revision.

### ELASTIC COEFFICIENT, $\gamma$

The equation[3] (page 313)

$$-\gamma \equiv -\frac{1}{v}\left(\frac{dv}{dp}\right)_T = \eta\left[\frac{41.38\ C_p}{pv} - \alpha_p\right] - \frac{T\cdot\alpha_p}{p}$$

has been used to calculate $\gamma$. (See Table V.) Since the values are obtained from measured small differences, they are of high precision, which is however difficult to determine. Hence an ample number of figures are given without any claim to an accuracy extending to the last figure. The reciprocals of the pressures are given in the last column to the right. $\gamma$ is everywhere less than $1/p$, the value for an ideal gas, and approaches it more closely at the higher temperatures and lower pressures. Helium is thus uniformly less compressible than the ideal gas which it resembles in this respect more closely at these temperatures and pressures.

### INTRINSIC ENERGY VARIATION WITH VOLUME, $\lambda$

$$\lambda \equiv (du/dv)_T = T\cdot\alpha_p/\gamma - p.$$

This equation[3] (page 315) was used to calculate $\lambda$. The values are given in Table VI. They are all very small and negative. This means that the intrinsic energy store at any fixed temperature decreases as the volume increases.

Table VII shows that $\lambda$ is sharply proportional to $p^2$. This has been predicted from van der Waals equation by using $\lambda = a/v^2$ and substituting for $v$ from $pv = RT$. Eq. (6) also shows that $\lambda : p^2$ since $(dp/dV)_T : p^2$.

TABLE VI. $-\lambda \times 10^2$ *in atm.*

| $p(m)$ | −50°C | 0°C | 50°C | 100°C | 200°C |
|---|---|---|---|---|---|
| 1 | 0.0021 | 0.0036 | 0.0056 | 0.0078 | 0.0077 |
| 5 | .052 | .091 | .090 | .191 | .194 |
| 10 | .21 | .37 | .49 | .79 | .79 |
| 20 | .83 | 1.51 | 2.34 | 3.13 | 3.15 |
| 30 | 1.85 | 3.36 | 5.28 | 7.07 | 7.08 |

TABLE VII. $-\lambda/p^2 \times 10^5$ *in* $(atm.)^{-1}$.

| $p(m)$ | −50°C | 0°C | 50°C | 100°C | 200°C |
|---|---|---|---|---|---|
| 1 | 1.16 | 2.19 | 3.46 | 4.62 | 4.62 |
| 5 | 1.22 | 2.14 | 3.31 | 4.51 | 4.51 |
| 10 | 1.16 | 2.19 | 3.41 | 4.62 | 4.62 |
| 20 | 1.11 | 2.18 | 3.44 | 4.62 | 4.62 |
| 30 | 1.11 | 2.18 | 3.44 | 4.63 | 4.62 |
| Average | 1.15 | 2.18 | 3.41 | 4.60 | 4.59 |

### $\eta$ AND $\lambda$, SECOND METHOD

A plot of $\lambda/p^2$ against temperature from Table VII and of $\eta$ against temperature from Table IV, showed that both $\lambda$ and $\eta$ go to zero at about −70°C. This suggested immediately that $\lambda$ and $\eta$ may be more simply related than indicated by the complex equations used for their calculation. Moreover, simpler methods for these calculations greatly facilitate the estimation of the effect of experimental error.

Let $\eta' \equiv (dT/dv)_u$ and $C_v$ be the specific heat at constant volume.

$$\eta' = -(du/dv)_T(du/dT)_v^{-1} = -\lambda/C_v$$

since

$$(du/dT)_v = (dq/dT)_v \equiv C_v.$$

Also

$$\eta' = -(dT/dp)_u(dp/dv)_u = \eta(dp/dv)_u;$$

$$\therefore\quad \eta = -(\lambda/C_v)(dv/dp)_u = -(\lambda/pC_v) \times [C_p\eta - T(dv/dT)_p]. \quad (3)$$

(See second paper[3] on air, p. 296, Eq. (1).)

$$\eta = \lambda T(dv/dT)_p[pC_v + \lambda C_p]^{-1}.$$

$\lambda C_p$ is small as compared to $pC_v$ even at low

pressures, so that with good approximation

$$\eta=(\lambda T/pC_v)(dv/dT)_p[1-K\lambda/p],\ K\equiv C_p/C_v. \quad (4)$$

Neglecting the small correction term, $K\lambda/p$, and obtaining $(dv/dT)_p$ from the equation for helium,[5] $pv=RT+bp$,

$$\eta=\lambda RT/p^2C_v \quad \text{or} \quad \lambda T/p^2\eta=\text{const.} \quad (5)$$

This is in good agreement with the results in the last column of Table VIII. Eq. (5) expresses the temperature dependence of $\lambda$ when the temperature dependence of $\eta$ is known.

TABLE VIII. *Relation between $\eta$ and $\lambda$.*

| $t$°C | $T$°K | $-\eta\times10^3$ | $-\lambda p^{-2}\cdot10^5$ | $\lambda p^{-2}T\eta^{-1}$ |
|---|---|---|---|---|
| −50 | 223.15 | 1.78 | 1.15 | 1.44 |
| 0 | 273.15 | 3.92 | 2.18 | 1.52 |
| 50 | 323.15 | 7.30 | 3.41 | 1.51 |
| 100 | 373.15 | 11.3 | 4.60 | 1.52 |
| 200 | 473.15 | 14.4 | 4.59 | 1.51 |

An examination of Eqs. (3), (4) or (5) shows that $\eta=0$ when $\lambda=0$, $p\neq0$, so that the curves of Fig. 2 should drop to zero at the same temperature. The experimental data, the kinetic theory discussed below and the thermodynamic relations indicate that $\eta$ does not go to zero at zero pressure. On the other hand, these indicate that $\lambda$ does become zero at zero pressure. This is not inconsistent with Eq. (3) above, since, for example, $(dp/dv)_u$ is approximately equal to $(dp/dv)_T$ which goes to zero at zero pressure.

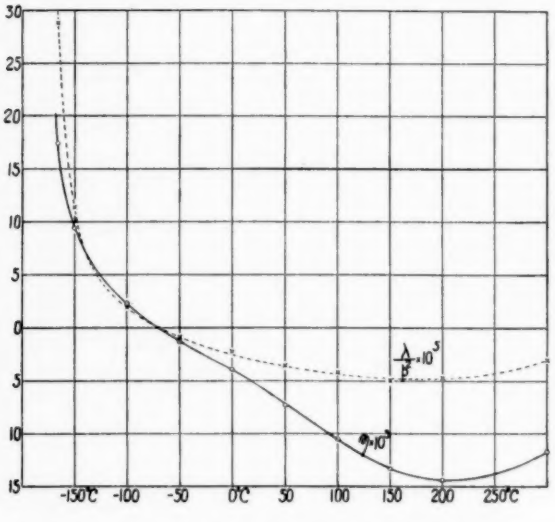


FIG. 2. $\eta$ and $\lambda/p^2$ as functions of temperature.

These equations, as do other thermodynamic equations, show that $\eta'$, as the definition of the coefficient of free expansion, would have led to simpler expressions than $\eta$. Also, it appears that $\lambda$ is a more fundamental thermodynamic quantity than either $\eta$ or $\eta'$.

It can be shown that

$$(dh/dp)_T=-\mu C_p$$

where $h\equiv u+pv$, the enthalpy. Hence,

$$-\mu C_p=(du/dp)_T+(dpv/dp)_T$$
$$=\lambda(dv/dp)_T+(dpv/dp)_T.$$

$$\therefore\quad \lambda=-(dp/dv)_T[\mu C_p+(dpv/dp)_T]. \quad (6)$$

When the experimental data used in the previous calculations for $\lambda$ were substituted into Eq. (6), values identical with the previous results were obtained for $\lambda$. The terms $\mu C_p$ and $b=(dpv/dp)_T$ (Table IX) are opposite in sign in the temperature range of these calculations and differ only a few percent in magnitude so that a small proportionate error in either of these terms introduces a larger proportionate error in $\lambda$. A plot of the $b$ values given by Holborn and Otto[5] against temperature shows that the point at 100°C falls above the curve by more than one-half percent. The irregularities of this curve and the variation of $C_p$ with temperature are the major sources of error in the preceding calculations leading to Tables IV and VII.

In Table IX the values of $\lambda/p^2$ in column 7 have been computed from Eq. (6) using the smoothed values of $b$, and, for the region below −49°C, using values of $C_p$ obtained by assuming a linear variation with temperature between the 18° and −180°C values given by Scheel and Heuse.[4] The difference between columns 6 and 7 at −50°C results from the different value of $C_p$ used, while at 100°C the difference arises from the different value of $b$ used. The values in column 7 are the more reliable.

$\lambda/p^2$ must ultimately decrease numerically with rising temperature, since in Eq. (6) $(dp/dv)_T : 1/T$. This decrease is already apparent in Fig. 2. However, consideration of the manner in which $\mu C_p$ enters Eq. (6) shows that the probable rise of $C_p$ with temperature would retard this decrease. At temperatures below −50°C, $\lambda/p^2$ begins to show pressure dependence,

TABLE IX. *Summary of $\eta$ and $\lambda$.*

| 1 | 2 | 3 | 4 | 5 | 6 | 7 | 8 |
|---|---|---|---|---|---|---|---|
| | $b$ | $b$ | | $b$ | | | |
| $t$°C | H.&O.[5] cal./g atm. | W.G.H.[6] cal./g atm. | $-\mu C_p$ cal./g atm. | smoothed cal./g atm. | $(+\lambda/p^2)10^5$ Table VII | $(+\lambda/p^2)10^5$ Eq. (6) | $+\eta\times10^3$ Eq. (5) |
| 300 | 0.06342 | | 0.07231 | 0.06365 | | −3.05 | −11.7 |
| 200 | .06685 | 0.06474 | .07769 | .06676 | −4.59 | −4.66 | −14.4 |
| 150 | | | .07806 | .06822 | | −4.69 | −13.3 |
| 100 | .06877 | .06832 | .07731 | .06956 | −4.60 | −4.19 | −10.5 |
| 50 | .07092 | .06913 | .07644 | .07073 | −3.41 | −3.56 | − 7.30 |
| 0 | .07159 | .07066 | .07456 | .07157 | −2.18 | −2.21 | − 3.91 |
| − 50 | .07207 | | .07331 | .07209 | −1.15 | −0.86 | − 1.29 |
| −100 | .07192 | | .07023 | | | 1.97 | 2.29 |
| −150 | .06891 | | .06195 | | | 11.4 | 9.41 |
| −183 | .06295 | | .05010 | | | 28.8 | 17.4 |

since for these low temperatures both $\mu C_p$ and $b$ vary with the pressure. For this reason $\lambda/p^2$ has been calculated in this region for one atmosphere.

$\lambda$ will later be used to calculate the Kelvin temperature of the ice point from the constant volume helium thermometer readings. In this connection an estimate of the error in $\lambda$ is desirable. This error is about 20 percent at 0°C and 12 percent at 100°C, or about 15 percent over the 0 to 100°C range.

The values of $\eta$ given in column 8 are calculated from $\lambda/p^2$ in column 7 by means of Eq. (5). The three low temperature values are consequently for one atmosphere. These values agree with those in Table IV obtained by a quite different method of calculation, except for the −50°C and 100°C points already discussed in connection with $\lambda/p^2$. This latter group of values of $\eta$ are probably the more reliable.

Columns 7 and 8 of Table IX have been used to plot the curves of Fig. 2. As previously pointed out, these curves must go through zero at the same temperature (−70°C), above which helium warms on free expansion. It is to be noted that there is a factor of 100 between the scales. In the temperature range of Fig. 2 the curves are similar in trend. At temperatures above those in the figure both $\eta$ and $\lambda/p^2$ appear to be going toward zero again. By combining Eqs. (5) and (6) one obtains

$$\eta = \text{const.}\ (\mu \cdot C_p + b). \qquad (7)$$

The percentage error in $\eta$ is therefore very nearly equal to that in $\lambda$ (see discussion following Eq. (6)). As discussed, this error is considerably larger than that in $b$ and $\mu C_p$ since $b$ and $\mu C_p$ are nearly equal numerically. Within the temperature range of Table IX both $b$ and $\mu C_p$ rise to a maximum and appear to be decreasing at approximately the same rate at the highest temperatures. Since this decrease is slow (6 percent in 100°C), Eq. (7) indicates that from these experimental data alone $\eta$ will decrease slowly with increasing temperature. The probable increase in $C_p$ with temperature should partially offset this decrease. It is, however, uncertain whether or not $\eta$ is decreasing at the highest temperature since the error in $\eta$ is here about 10 percent. This analysis of $pv$ and porous plug data then suggests that at the highest temperature the curve for $\eta$ will depart from the horizontal more slowly than in Fig. 2.

A comparison of Eqs. (6) and (7) shows that since $(dp/dv)_T : 1/T$, the curve for $\lambda/p^2$ should go toward zero faster than that for $\eta$ by the factor $1/T$.

## APPLICATION TO KINETIC THEORY

It will be shown here, as a direct deduction from the preceding experimental data, that the behavior of helium on free expansion is determined by the changes which occur in the total potential energy of collision of the mass of atoms when free expansion takes place. The general form of the deduced law of force is of the type deduced elsewhere[7] from considerations of the quantum theory.

Kinetic theory explanations of the large cooling of a gas on free (Joule) expansion as, for example, with air, have necessarily to be based

[6] Wiebe, Gaddy and Heins, J. Am. Chem. Soc. **53**, 1721 (1931).

[7] Penney, Phys. Rev. **42**, 585 (1932).

on the presence of attractive forces against which work is done at the expense of the store of kinetic energy. The free expansion coefficient for air is a marked function of the volume and hence these forces cannot be negligible at distances of the order of the mean free path.

Since helium warms on free expansion, one thinks first of the possibility of these forces being repulsive. For helium the value of $\eta$ is independent of the pressure. That is, at any one temperature,

$$\eta \equiv (dT/dp)_u = K_1.$$

If $C_p$ is also constant,

$$C_p \cdot \Delta T = K_2 \cdot \Delta p = F \cdot \Delta x.$$

Hence for a fixed $\Delta p$ the energy involved is a constant independent of the pressure. $F$ is the repulsive force and $\Delta x$ is the change in the average separation due to the $\Delta p$ and in which it is assumed that the work done by $F$ over $\Delta x$ supplies the $(C_p \cdot \Delta T)$ energy. Noting that $\Delta v = K_3 x^2 \cdot \Delta x$ and $pv = \text{const.}$ one finds that $F : x^{-4}$. This result is not in agreement with similar expressions resulting from measurements on viscosity[8] and from considerations of the quantum theory,[7] which lead to higher negative powers.

Moreover, the data above show that $\eta$ decreases and changes sign with falling temperature, while remaining independent of the pressure and therefore of the volume, for the major part of the range. This requires these forces to be a function of the velocity of the molecules even to the changing of sign. The assumption of this type of repulsive force is thus quite untenable.

Dr. R. Rollefson of our laboratory suggested that the collision energy in the gas may need to be taken into account. During a collision the colliding molecules decrease their kinetic energy by the amount necessary to supply the required work against the repulsive forces. This provides a means by which the energy of the gas may be shifted between potential and kinetic forms by variation of the collision velocity and of the number of collisions in progress at any instant. As will presently appear, the assumption of repulsive forces extending over a small part of the mean free path permits a qualitative explanation of the observed behavior of $\eta$ for helium and avoids as well the impass discussed in the preceding paragraphs.

In the simple kinetic theory where the molecules are treated as highly elastic spheres with hard sharp boundaries, the time of collision is made extremely short. While the maximum energy store per collision is the same, the number of collisions in progress at any instant is made small enough that for the purpose in hand the potential energy involved may be neglected.

Since there are no forces acting between the helium molecules at their average separation, change of this separation does not involve work and there will be no free expansion effect from this cause. The number, $z$, of collisions in progress at any instant in a fixed mass of gas at a given temperature is proportional to the density and hence to the pressure, since Boyle's law holds to a good approximation. Therefore $\Delta z/\Delta p = K$, a constant. If $\epsilon$ is the average potential energy of a collision, then $\epsilon \Delta z$ is the change in potential energy. In a free expansion at a fixed initial temperature, with a given pressure drop, $\Delta p$,

$$\epsilon \Delta z = K\epsilon \cdot \Delta p.$$

Where only repulsive forces are present, $\epsilon \Delta z$ is a decrease in the potential energy which appears in the kinetic form by an amount $C_v \cdot \Delta T$, where $\Delta T$ is the observed rise in temperature. Then

$$-\epsilon \cdot \Delta z = -K\epsilon \cdot \Delta p = C_v \Delta T.$$

$$\therefore \quad (\Delta T/\Delta p)_u \equiv \eta = -K\epsilon/C_v.$$

Hence in such a free expansion $\Delta T$ is proportional to $\Delta p$ since for helium $C_v$ and $\epsilon$ are constant and Boyle's law is obeyed. Thus $\eta$ should be independent of the pressure and be of negative sign. This is in agreement with the experimental data of Table IV.

The above argument relating to the independence of $\eta$ on the pressure can be expected to hold only if the average molecular separation, even at the highest pressures, exceeds greatly the range of the repulsive force.

The number of collisions in progress at any instant and the character of these collisions are both functions of the temperature. The number of collisions per molecule at a fixed volume will to a first approximation be proportional to the

[8] Lennard-Jones, Proc. Roy. Soc. **A107**, 157 (1925).

average velocity of the molecules, that is, proportional to the square root of the Kelvin temperature. On this account $\eta$ would become larger numerically with rising temperature.

The number of collisions at any instant at any temperature will depend also on the duration of the individual collision as a function of the temperature. It is not evident, without a general solution of the collisions as a two body problem, whether the above function increases or decreases with the temperature.

In general, the average potential energy per collision, $\epsilon$, is an increasing function of the temperature since the depth of penetration is increased at higher molecular velocities. For the special case of the head-on collision in which both colliding molecules come to rest, the potential energy increases as the absolute temperature.

These considerations would lead one to expect that $\eta$ should increase in absolute value more rapidly than the first power of the absolute temperature. Consideration of the data for $\eta$, Table IV, shows that it is very approximately proportional to $(T-163)^{1.33}$ for temperatures above $-50$°C.

The values of $\eta$ from Tables VII and IX are plotted against temperature in Fig. 2. The curve crosses the zero axis at $-70$°C and rises rapidly thereafter. This corresponds with the observed behavior of air[3] for which $\eta$ decreases rapidly with rising temperature, passing, undoubtedly, through zero at a somewhat higher temperature.

If there be added to the repulsive force field about the molecule an attractive field decreasing much less rapidly with distance, then as a pair of molecules approach each other they pass first through an attractive force field, with increasing velocity, and into the repulsive field where their approach is stopped. For high speeds of approach the loss in potential energy in the attractive field is relatively small, and the time spent there is also small, so that the contribution to the total instantaneous energy of collision is small. But as the molecular speed is reduced the depth of penetration for glancing collisions will increase on the average, thus increasing the contribution of those collisions which do not approach near enough for the repulsive field to act, and at the same time increasing the average time spent in the attractive field. Thus as the molecular speed is reduced, the subtraction of the attractive field from the potential energy of collision at any instant increases both from the increasing energy of the glancing collision and from the longer time spent in the attractive field. Simultaneously, the contribution of the repulsive field is falling due to the fall in molecular velocity. Thus the collision energy decreases more rapidly than the temperature. Evidently $-C_v \cdot \eta$, the ratio of the collision energy change to the pressure change, will move rapidly toward zero with falling temperature and finally become positive.

As this condition is approaching, $\eta$ must become a function of the pressure, and its temperature dependence become still more complicated, since finally all the molecules are continually in the state of collision, that is, continually within the range of each other's force field.

The mutual potential energy between two helium atoms as a function of their distance of separation has been calculated from the quantum theory. The results are summarized by W. G. Penney[7] and have been used by Kirkwood and Keyes[9] as the foundation of an equation of state from which they calculate with considerable success a number of properties of helium. This mutual potential energy appears as the sum of two terms, both of which drop off rapidly with atomic separation but much the more rapidly for the positive term due to the force of repulsion. The repulsive force field thus forms a core surrounded by an attractive force field. This is obviously in agreement with that postulated above to explain the behavior of $\eta$.

The above collision hypothesis predicts the pressure behavior of $\lambda$ as appears from the following argument. If $z$ represents the number of collisions in a given mass of gas at any instant, it has been shown above that at constant temperature $z : p$. Hence, where $\epsilon$ is the average energy per collision,

$$(\epsilon dz/dp)_T = \text{const.} = (du/dv)_T (dv/dp)_T$$
$$= -\lambda v/p = -\lambda K/p^2$$

since Boyle's law is closely obeyed by helium. Hence $\lambda : p^2$ on this collision hypothesis. This agrees with the data of Table VII.

[9] Kirkwood and Keyes, Phys. Rev. **37**, 832 (1931).

## Perfect Gas Theory

A perfect gas is usually defined as one for which $(pv)_T = \text{const.}$ and $\eta = 0$. The experimental observations that Boyle's law holds exactly at sufficiently low pressure and, that Boyle's law holds better at higher temperatures, have led to the conclusion that any gas becomes a perfect gas at sufficiently low pressures and high temperatures. The above conditions are satisfied most nearly by helium.

When $\mu$ and $\eta$ are calculated from $(pv)$ and specific heat data alone, they appear as small differences between much larger experimental quantities. The magnitudes and trends of these small differences prove to be too unreliable for testing the departure of helium from the condition $\eta = 0$. Direct experimental measurements on either $\mu$ or $\eta$ have not been available. As a result, statements regarding the manner in which a real gas approaches ideality have been based entirely upon its $pv$ behavior.

The above data for helium show that $\eta$ is independent of pressure to the extent that $\mu C_p$ and $b$ are also. Above 0°C the latter are experimentally independent of the pressure in the range 1–40 atmospheres. Since there are no obvious reasons for supposing that this pressure independence should not continue indefinitely below one atmosphere, it appears that, contrary to the usual conclusion from its $pv$ behavior, helium does not become a perfect gas at low pressure.

Neither the data nor the preceding kinetic theory gives any clear support to the hope that, on the other hand, $\eta$ will go to zero at some still higher temperature and thus satisfy the conditions for ideality. This appears from the above analysis of the data for $\eta$. Thus the departure of the curve for $\eta$, Fig. 2, from horizontality is first very slow and, second, somewhat open to question. Further, granting that the upward trend of the curve is actual, it must approach the axis asymptotically in order to satisfy the ideality demand. In the latter event, the temperature at which $\eta$ can become vanishingly small is very high. The kinetic theory discussed earlier in this paper predicts the pressure behavior quantitatively, and the prediction is in excellent accord with the observations. The theory predicts the temperature behavior qualitatively, and is in general agreement with the observations. There is no factor in this theory which tends to diminish the numerical value of $\eta$ above 0°C. On the contrary, the theory shows that $\eta$ should continue to increase numerically with increasing temperature.

In conclusion, there appears to be an experimentally measurable limit in the approximation of helium to a prefect gas state at any pressure or temperature.

The helium used in these experiments was supplied by the Bureau of Mines of the United States Government. We regret that by oversight this statement was omitted from the first paper on helium.[1] Their cooperation in the matter made this experimental work possible, and we have appreciated it very greatly.

It is a pleasure to acknowledge the help given this work by grants from the Wisconsin Alumni Research Foundation.

In a following article, the data on $\mu$ and $\lambda$ will be used to calculate the value of the ice point on the Kelvin scale from the available gas thermometer data.

# LETTERS TO THE EDITOR

*Prompt publication of brief reports of important discoveries in physics may be secured by addressing them to this department. Closing dates for this department are, for the first issue of the month, the twentieth of the preceding month; for the second issue, the fifth of the month. The Board of Editors does not hold itself responsible for the opinions expressed by the correspondents.*

## The Free Mobility of Lead Ions in Amicronic Crystals of Lead Sulfate

In certain of our studies of structural changes taking place upon aging of freshly formed crystalline precipitates we mixed 0.1 molar solutions of lead nitrate with 0.1 molar solutions of potassium sulfate at room temperature. The freshly formed lead sulfate was seen to be distinctly crystalline under the microscope, the size of the particles being of the order of 0.5 to 1 micron in width and 1 to 2 microns in length. The external surface of the particles could be calculated from these dimensions as well as from the amount of wool violet (4BN) which was adsorbed when the surface was saturated with the dye. On aging, the size of the particles as observed under the microscope hardly changed; correspondingly the total external surface decreased relatively slightly after one day of aging. By making use of the distribution of thorium B—a radioactive isotope of lead—between the solution and the crystalline precipitate (method of F. Paneth), it was shown that the freshly formed precipitate had an enormous internal surface which was accessible to lead. As a matter of fact the thorium B distributed itself homogeneously throughout the *entire* crystalline precipitate when the latter, immediately after its formation, was shaken for 3 minutes with a radioactive lead solution. During aging, the internal surface of the precipitate decreased rapidly as a result of a perfection process occurring inside the microscopic crystals. It was found that at room temperature the internal surface, as calculated from the adsorption of thorium B after one minute of shaking with the precipitate, corresponded to 220 mg of lead per 1 g of lead sulfate very soon (one minute) after precipitation, and to 5.8 mg after aging for 50 minutes. In spite of this rapid decrease of the internal surface it was found that the thorium B could distribute itself homogeneously throughout the fifty minutes old precipitate if the mixture was shaken for seventeen hours with the radioactive isotope. The experiments have been repeated with radioactive precipitates and the effusion of thorium B studied on aging. The same effects were observed as with the inactive precipitates.

X-ray pictures, made at our request by Dr. E. J. W. Verwey at the University of Groningen (Holland), showed that a precipitate less than fifteen minutes old gave the same lines as well-aged lead sulfate. The fresh precipitate, however, gave very diffuse lines, and it was estimated that the primary particles contained at least 1000 to 10,000 molecules. This approximation is very rough and we plan to study this point in greater detail.

From the above it is clear that the freshly formed microscopic crystals of lead sulfate have a spongy structure. They consist of primary crystalline particles separated by fine capillaries with a diameter of the order of molecular dimensions. Thorium B ions can move freely to the internal surface but the capillaries are too fine to allow a diffusion of the dye (wool violet) into the interior. On aging a perfection process occurs in the interior of the crystals, resulting in a growth of the primary particles and a decrease of the internal surface. *The most striking result of this study, however, is that lead ions can move freely through the primary particles and cause a homogeneous distribution of the thorium B through the entire system. Thus we are led to the conclusion that lead ions can move freely through the amicronic primary particles.* On aging this free mobility decreases with the growth of the primary particles, but even in a precipitate fifty minutes old, a homogeneous distribution of thorium B is found on longer shaking.

A more detailed account of all the experimental work and its interpretation will be presented in subsequent communications to the *Journal of the American Chemical Society.*

I. M. KOLTHOFF
CHARLES ROSENBLUM

School of Chemistry,
University of Minnesota,
February 9, 1934.

## Continuous Electron Radiation in Gas Discharges

One group of continuous gas spectra has not been explained up to the present time, namely the continuous spectra emitted by all condensed discharges. To this group belongs especially the continuous background of all condensed sparks. Extreme types of these spectra are the continuous underwater spark spectrum, the spectrum of the exploded wires and the continuous spectrum emitted by high current vacuum sparks. All these spectra are in spite of their apparent difference phenomena of the same kind. That becomes evident from a comparison of the properties of the spectra.

Total intensity and intensity distribution of all these

continuous spectra are to a first approximation *not* dependent in the individual material of the electrodes and the medium, in which the discharge takes place. The intensity of all these continuous spectra increases with increasing current density, i.e., by increasing the spark energy (capacity or voltage), by confining the discharge to a smaller diameter, and by shortening the duration of the spark by reducing self-induction and Ohmic resistance or by increasing the pressure. In the spectra of the vacuum spark and of the exploded wires a continuous absorption has been found proportional to the current density. The other sparks have not yet been studied with respect to this phenomenon. All these continuous spectra are emitted only in that stage of the spark where we expect highest current and ion density. They appear always together with very broad spark lines and disappear in the later stages with decreasing broadening of the lines.

We conclude from these common properties of all the continuous spark spectra arising under such different discharge conditions that their origin must be due to the same process. There seems to be only one possibility: the radiation of free electrons in the field of the positive ions formed in the discharge, or in terms of the Bohr theory the transitions between hyperbolic orbits.

The properties which we expect from the theory for the continuous electron radiation are in best agreement with the observed properties of the continuous spark spectra. The intensity of the electron radiation is proportional to the number of collisions between electron and ions, i.e., proportional to the current density and the ion density which is determined by current density and applied voltage. The radiation is consequently to a first approximation independent of the individual properties of the ions involved. In agreement however with the experimental results we expect a small individual influence of the different ionization potentials of different elements, especially in the case of very low electron velocities due to transitions between hyperbolic and elliptic orbits. Since transitions between continuous energy levels take place in both directions, a continuous absorption must be connected with the continuous emission, in agreement with the observations on the exploded wires and the high current vacuum sparks. Since the continuous radiation is dependent on the ion density, we expect in connection with the continuous radiation the emission of spark lines, broadened by a Stark effect due to the field of the surrounding ions. Here we have also agreement between theory and observation. This agreement and the fact that there is no other possibility to explain the properties of the observed continuous spectra, seem to be a very strong argument for our explanation.

A quantitative comparison of the theoretical and experimental intensities is still impossible, because there are no exact measurements of the intensity under various excitation conditions, and the theoretical calculation is difficult because we have no exact figures for the ion density during the whole time of the spark emission. A rough calculation, however, shows that at least the order of magnitude of observed and theoretical intensity seems to be in agreement.

A detailed treatment of the problem will appear in the *Zeitschrift für Physik*.

WOLFGANG FINKELNBURG*
Norman Bridge Laboratory of Physics,
California Institute of Technology,
February 3, 1934.

* Fellow of the Rockefeller Foundation.

## Large Barkhausen Discontinuities and Their Propagation

While investigating the relationship between the velocity of propagation of large Barkhausen discontinuities and longitudinal field for various fixed values of tensile stress for 10 percent Ni-Fe alloy wires, it was observed that the shift of the velocity-field characteristics relative to the field axis with change in tensile stress corresponded rather accurately to the change in height of the hysteresis loop with change in tensile stress. Both of these changes were observed to saturate with tension, i.e., for high values of tensile stress a given change in tension produces a smaller shift of height of hysteresis loop or of shift of velocity-field characteristic than does the same change in tension for a lower value of tensile stress. Further, for a 70 percent Ni-Fe wire, the height of the hysteresis loop changes but little with changes in tension, and also the velocity-field characteristics shift but little with tension changes. Again, for a pure nickel wire under torsion, more qualitative indications of the dependence of the velocity of propagation upon the intensity of magnetization were observed. An increase in tension for a nickel wire under torsion caused a shift of velocity-field characteristics to higher field values while the height of the hysteresis loop was found to decrease. This is just the reverse of the case for the two alloys mentioned above for which an increase in tension was found to shift the velocity-field characteristics to lower field values and to increase the height of the hysteresis loops.

Because of such qualitative indications of the relationship between velocity and height of hysteresis loop or between $v$ and $I$ the quantitative relation existing between $v$ and $I$ was investigated. A velocity *versus* $I$ curve was obtained for a 10 percent Ni-Fe wire by holding $H$ constant and varying $I$ by means of varying the tensile stress. The $v$ *versus* $I$ curves obtained in this manner were found to be similiar in form to $v$ *versus* $H$ curves.

In a paper now in the hands of the publishers, the author has presented evidence for a 10 percent Ni-Fe alloy that in general for any strain produced by tension and torsion combined, it is only the component of field in the direction of maximum strain which influences the velocity. That is, in general, the field effecting propagation is $H \cos \theta$, where $H$ is the applied field, and $\theta$ the direction the field makes with the direction of maximum elongation. Upon considering this relation in connection with the observations relative to $I$ presented above, one might infer that the

velocity might be a function of $HI\cdot\cos\theta$ only, since this satisfies the condition required above that the functional relation between $v$ and $I$ be the same as between $v$ and $H$, and also the relation between velocity and $H\cdot\cos\theta$.

The possible relationship between $v$ and $HI\cdot\cos\theta$ can be most easily tested in the case of pure tension. Here $\cos\theta=1$ and $v$ should depend upon the product $HI$ only. Table I shows the values of $H$, $I$ and $HI$ for a 10 percent

TABLE I.

| Tensile stress Kg/mm² | $H$ Oersteds | $I$ c.g.s. units | $HI$ |
|---|---|---|---|
| 25.2 | 4.80 | 1072 | 5149 |
| 28.8 | 4.51 | 1140 | 5148 |
| 32.4 | 4.27 | 1190 | 5080 |
| 37.2 | 4.03 | 1270 | 5120 |
| 42.0 | 3.84 | 1316 | 5057 |
| 46.8 | 3.68 | 1365 | 5030 |
| 51.6 | 3.55 | 1410 | 5005 |
| 57.6 | 3.40 | 1453 | 4940 |
| 63.6 | 3.30 | 1483 | 4897 |
| 72.0 | 3.27 | 1494 | 4882 |

Ni-Fe wire. The data are for a constant velocity of 6500 cm/sec. The values of $I$ were not corrected for changes in area of the wire with tension. The small change in the product $HI$ could thus easily be accounted for.

Since the velocity of propagation seems to be a function of $I$, it must be related to the magnetostrictive properties also since the relationship between $I$ and magnetostriction has been rather well established. The relationship between $v$ and the field component in the direction of maximum elongation was established for the 10 percent Ni-Fe alloy for which the magnetostriction is positive. The relationship between $v$ and the component of field in the direction of maximum strain was investigated for pure nickel for which the magnetostriction is negative. For pure nickel under torsion and tension the velocity was found to depend only upon the component of field in the direction of maximum compression. For negative magnetostriction, then, the preferred direction of orientation is along the compression axis, while for positive magnetostriction it is along the direction of maximum elongation. This leads to an understanding of why in one case the observed hysteresis loop increases with tension and in the other case decreases. In the case of positive magnetostriction the magnetic vector rotates into the direction of the wire axis with increasing tension, while in the case of negative magnetostriction it rotates away from the direction of the wire axis. Actually, the effects of tension upon the direction of preferred orientation seem to be analogous to the effects, for example, of pressure on melting point. For those alloys which tend to increase in length when being magnetized a mechanical lengthening aids the magnetizing, while for the others the reverse is true.

Investigations into the possible relationship between $v$ and $HI\cdot\cos\theta$ are contemplated in the case where wires are subjected to both tensile and torsional stresses.

RAYMOND E. REINHART

University of Kansas,
February 2, 1934.

## On the Theory of the Electron and Positive

To the paper appearing in the February 15 issue of this journal under the same title we wish to add a few further considerations. In particular the discussion of the gauge invariance of the formalism there given is incomplete, and these supplementary remarks may help to clarify the question of the proper interpretation of the theory.

(a) The solutions $\psi_{N,M}(r;\rho)$ of the wave equation (2.32) are not independent of the choice of gauge to represent the electromagnetic field. In particular the quantities

$$\sum_{r}\sum_{\rho}\bar{\psi}_{N,M}(r;\rho)\psi_{N,M}(r;\rho),$$

which give the probability of finding just $N$ electrons and $M$ positives in the system, are gauge dependent, and this gauge dependence is not directly connected with the divergence of the sums. Thus the vanishing of a $\psi_{N,M}$ can be given no physical meaning; and the vanishing of all the $\psi_{N,M}$'s except $\psi_{00}$, though a sufficient condition for the vanishing of the charge and current density everywhere, is not a necessary one. From this it follows that the number of particles in a system can be given no unambiguous physical meaning, except in those limiting cases in which one may abstract from that creation and destruction of particles which characterizes the relativistic quantum theory.

(b) The operators which represent the physical variables of the system, such as the charge and current density, the kinetic energy, the mechanical momenta $\mathbf{p}-(e/c)\mathbf{A}$, and their rate of change with time, are, formally, gauge invariant. The proof of this, which is based, in complete analogy to the proof of relativistic covariance, on the invariance of the Dirac equations and of the spurs (2.26), depends however on the assumption of the convergence of all sums.

(c) In fact the sums met with in the theory do not in general converge, and by the subtraction of the spur (2.26) their terms are automatically rearranged. Thus in practice we find that the operators representing, say, charge and current are gauge dependent; for the same reason they may depend in noncovariant manner on the choice of Lorentz frame. This point is very forcibly illustrated by considering the transformation from the constant potentials

I $\qquad \mathbf{A}=0, \quad V=V_0$

to

II $\qquad A_x=\sinh\beta\cdot V_0, \quad A_y=A_z=0, \quad V=\cosh\beta\cdot V_0,$

which may be regarded either as a gauge or Lorentz transformation. Whereas the expectation value of the $x$-component of the current density vanishes for the potentials I, it is infinite for II.

(d) Under these circumstances it is essential to distinguish between those results of the theory which can be unambiguously computed and those which cannot. In general all the results of the theory which are given by convergent expressions—the energy differences in a given field, the rate of production of pairs, the transition probabilities—are gauge and Lorentz invariant; but this is not true of those predictions which, like the treatment of the (0) state in Section 4, depend essentially on the reaction of pairs of arbitrarily high energy. As is more fully discussed in that section, these divergence difficulties are closely connected with the inadequacy of quantum theoretical field methods when applied to very short lengths, and are of such a character that the predictions of the theory, even if they could be computed unambiguously, could not be unambiguously compared with experiment. It therefore seems possible that no sensible improvement in the theory will be made on the basis of the present quantum theoretical treatment of fields; certainly no obvious changes in the definition of positive and negative states overcome the difficulties here formulated.

(e) We are indebted to Professor Breit for pointing out to us that the proofs leading up to (3.2) and (3.14), which establish the validity of the use of the Dirac equation for computing energy differences and matrix elements, can be greatly simplified. For the formalism on which the proofs are based differs from the quantum mechanical formalism of a many body problem only by the subtraction of the spur (2.26), and in this latter formalism the equalities (3.3) and (3.14) follow directly from the transformation theory. But on the quantities involved here, namely the nondiagonal elements of an operator, and the differences between various diagonal elements, the subtraction of the spur, which in no way involves the dynamical variables of the system, can have no effect.

W. H. Furry
J. R. Oppenheimer

Berkeley, California,
February 12, 1934.

## The Surface Ionization of Potassium on Tungsten

The surface ionization of alkali metals on W and W—O surfaces partly covered by adsorbed layers of the alkali metal has been investigated by Langmuir[1] and others.[2, 3, 4] The method employed by them involved surrounding the ionization unit with the saturated vapor of the alkali metal. Attempts by these investigators to extend measurements to high temperatures have not been successful because of the onset of large photoelectric currents from collector to wire at about 1500°K.

While observing the scattering of a ray of potassium atoms from a crystal surface, we employed a tungsten wire and collector cylinder as a detector.[1, 5] With the detector surrounded by liquid air, no evidence of a photoelectric current was observed even at high wire temperatures. This suggested the use of a molecular ray method to determine the efficiency of surface ionization of potassium by tungsten at high temperatures.

A potassium ray of constant intensity was allowed to fall upon a clean tungsten wire in an extremely high vacuum, and the positive ion current was measured at several wire temperatures. Without disturbing the ray, the wire was then covered with oxygen, and the positive ion current obtained was assumed[1] to correspond to 100 percent ionization. The circled points in Fig. 1 show the results of an experiment in which the vacuum conditions were unusually good.

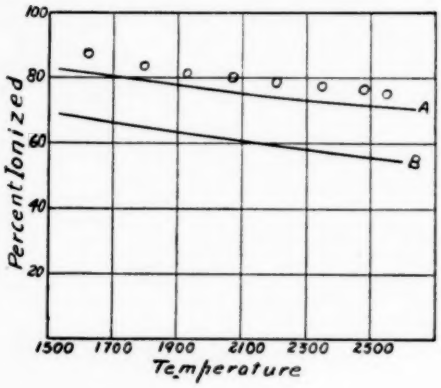


FIG. 1.

The chief interest in the results lies in the fact that all of the preliminary data are clustered about a theoretical curve (Fig. 1, *A*) calculated by omitting the ratio of statistical weights from the modified Saha equation. This equation may be written

$$\nu_+/\nu_a=(\omega_+/\omega_a)\exp\left[-(I-\phi)\epsilon/kT\right], \qquad (1)$$

in which $\nu_+$ is the number of ions and $\nu_a$ the number of atoms of ionization potential $I$ evaporating per second from 1 cm² of a surface of work function $\phi$ at temperature $T$; and $\omega_+$ and $\omega_a$ are the statistical weights. In calculating theoretical percents ionized, the following values were assumed for the constants: $\phi$ (tungsten) = 4.52 e. v.; $I$ (potassium) = 4.32 e. v.; and $\omega_+/\omega_a=\frac{1}{2}$. Fig. 1, *B* gives the theoretical percent ionized as a function of temperature when the statistical weights' ratio $\frac{1}{2}$ is included. It is evident that the experimental results are in better agreement with *A* than with *B*. However, there seems to be no justification for the omission of the statistical weights from Eq. (1).

A clue to the cause of the divergence between the experimental points and theory appears when the data are plotted to the axes log $(\nu_+/\nu_a)$ against $1/T$, as is done in Fig. 2. Since $\omega_+/\omega_a$ is 0.5, an intercept equal to log 0.5, or

[1] I. Langmuir, Proc. Roy. Soc. **A107**, 61 (1925).
[2] Ives, Phys. Rev. **21**, 385 (1923).
[3] Meyer, Ann. d. Physik (5) **4**, 357 (1930).
[4] Becker, Phys. Rev. **28**, 341 (1926).
[5] Taylor, Zeits. f. Physik **57**, 242 (1929).

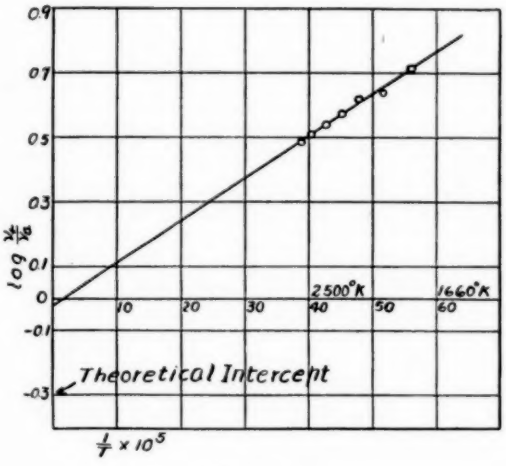


FIG. 2.

$-0.30$, is to be expected. The experimental data, however, exhibit an intercept of about $-0.03$. Several other preliminary experiments have led to intercepts which lie both above and below the origin, but within the limits $\pm 0.1$. These observations point to the possibility that a factor, which multiplies the exponential term and cancels at least in part the statistical weights' ratio, has been omitted in Eq. (1). A somewhat more general equation may be written, which contains such a factor, involving reflection coefficients for ions and atoms, namely,

$$\frac{\nu_+}{\nu_a} = \frac{1-r_+}{1-r_a} \cdot \frac{\omega_+}{\omega_a} \exp\left[\frac{-(I-\phi)\epsilon}{kT}\right]. \qquad (2)$$

If the ratio $(1-r_+)/(1-r_a)$ were equal to approximately 2, the absence (within experimental error) of an intercept would be accounted for. There are at present no experimental data upon the reflection coefficients of atoms or ions known to the writers. It has been assumed in the past that the ratio $(1-r_+)/(1-r_a)$ is nearly unity.

It may be significant that the dilemma which arises here is very similar to that which arose recently in the case of the thermionic emission of electrons,[6] and which led to the suggestion of a reflection coefficient for electrons of $\frac{1}{2}$. It will be apparent from the discussion above that very careful work would be necessary in order to establish or disprove the existence of zero intercept.

It should be stated here that the above experiment affords a method for the determination of the work function of tungsten independent of thermionic emission. The value of $\phi$ obtained from the slope in Fig. 2 is 4.56 e.v. Several other determinations have given values ranging from 4.50 to 4.57 e.v.

M. J. COPLEY
T. E. PHIPPS

Department of Chemistry,
University of Illinois,
February 5, 1934.

[6] See Fowler, *Statistical Mechanics*, p. 268, Cambridge Press (1929).

## Gamma-Rays from Carbon Bombarded with Deutons

By using the method previously applied[1] to other elements we have observed a very penetrating radiation from carbon bombarded with deutons, and have attempted to analyze it. We have made measurements of the absorption of this radiation in lead and in paraffin, with two electroscopes, one lined with lead and the other with paraffin. The tube was operated at 900 kilovolts and 10 microamperes ion current. The hydrogen contained about 30 percent $H^2$. The ions were allowed to impinge alternately on a target of graphite and a target of some heavier element. Aluminum, copper and tantalum were tried, with the same hydrogen and also with ordinary hydrogen, and found to give readings which were practically identical among themselves and were presumably due to stray x-rays plus the residual ionization of the electroscope. These readings were taken as the background to be subtracted from the total effect obtained with the graphite target, and the difference was ascribed to the products of a reaction involving carbon and $H^2$.

The ionization produced in the lead-lined chamber was about 1.4 times that produced in the paraffin-lined chamber under the same conditions, which is approximately the ratio found for $\gamma$-rays. We have also compared the absorption in paraffin with the absorption in lead and found 25 mm of paraffin to be equivalent to less than 3 mm of lead. Both of these results indicate that neutrons are not

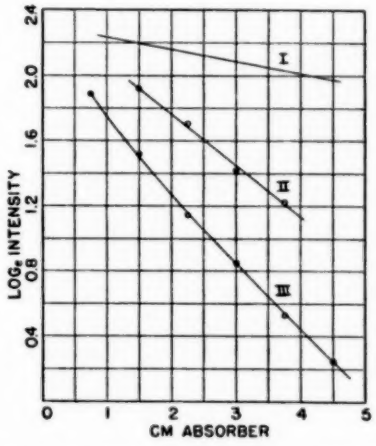


FIG. 1. Absorption in lead of I, neutrons; II, C+$H^2$ radiation and III, thorium $\gamma$-radiation.

present in sufficient numbers or with sufficient energy to be detected under the conditions of our experiment. We conclude therefore that the ionization is produced by very hard $\gamma$-rays.

[1] Crane, Lauritson and Soltan, Phys. Rev. **44**, 514 (1933).

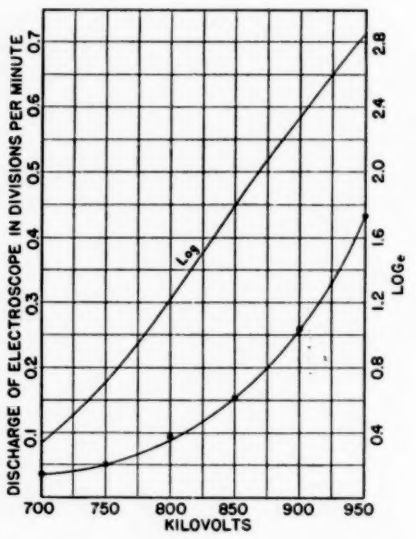


FIG. 2. Intensity of radiation as a function of accelerating voltage, after 1.5 cm lead filtration.

By comparing the absorption curve for the $C+H^2$ radiation in lead (Fig. 1, curve II) with the curve for the absorption of $\gamma$-rays from thorium (curve III) obtained with the same experimental arrangement, we find that the radiation from $C+H^2$ is considerably more penetrating. For thorium we find the apparent absorption coefficient in lead to be 0.42 $cm^{-1}$, while the true absorption coefficient is 0.478 $cm^{-1}$. This indicates that scattered radiation introduces an error of approximately 13 percent. For the $C+H^2$ radiation the apparent absorption coefficient is 0.31 $cm^{-1}$, and if we apply the same correction of 13 percent as in the case of thorium, this gives $\mu=0.35$ $cm^{-1}$ as the most probable value. It is somewhat uncertain to what quantum energy this absorption coefficient corresponds, but it is probably in the neighborhood of $3.5\times10^6$ e.v.

By comparing the intensity of ionization produced by the $C+H^2$ radiation with that from a known quantity of radium we find our source to be approximately equivalent to $2.5\times10^{-6}$ gram of radium. This amount of radium produces about $2\times10^5$ quanta per second, and allowing for the smaller absorption of our radiation in the ionization chamber, we estimate that we are producing roughly $3\times10^5$ quanta per second. Assuming that our beam contains $10^{13}$ $H^2$ ions per second which have velocities near the maximum, this means that three quanta are produced per $10^8$ $H^2$ ions. Due to the much smaller absorption coefficient of neutrons in lead (indicated by curve I, Fig. 1) an appreciable number of neutrons could not escape detection, and we estimate that the number of neutrons present is less than one-fifth the number of quanta.

Lawrence, Livingston and Lewis[2] find protons having a range of 18 cm when they bombard carbon with deutons of $1.3\times10^6$ e.v. It would seem reasonable to associate the $\gamma$-rays which we observe with these protons. If this is correct the most probable process appears to be

$$C^{12}+H^2\rightarrow C^{13}+H^1+\gamma.$$

If we use the following values in mass units:

| | |
|---|---|
| $C^{12}=12.0036$ | kinetic energy of $H^2=0.0010$ |
| $C^{13}=13.0039$ | $H^1=.0030$ |
| $H^1=1.0078$ | $C^{13}=.0002$ |

we obtain $12.0036+2.0136+0.0010=13.0039+0.0002+1.0078+0.0030+\gamma$. This gives $\gamma=0.0033$ mass units, or $3.1\times10^6$ e.v., which agrees within the experimental uncertainty with the estimate made from our absorption measurements, and leads us to believe that the process here suggested is correct.

It is a pleasure to acknowledge our indebtedness to the Seeley W. Mudd Fund for the support of this work.

C. C. LAURITSEN AND H. R. CRANE

Kellogg Radiation Laboratory,
California Institute of Technology,
February 15, 1934.

[2] Lawrence, Livingston and Lewis, Phys. Rev. **44**, 56 (1933).

## Measurement of the Townsend Coefficients for Ionization by Collision—Additional Data

It has been brought to the writer's attention that in two recent papers[1] on the values of the Townsend coefficients in air, no mention was made of the temperature at which the measurements were carried on. The temperature is of considerable importance as the coefficient $\alpha$ is actually a function of $X$/(gas density) rather than $X$/pressure ($X$ = field strength in volts/cm). All measurements were conducted in a room of sensibly constant temperature, the average being 22°C and the deviation above or below this value less than 1°C. This gives a maximum allowable error in the absolute temperature, and hence in the gas density, of about 0.3 percent. The maximum error in the case of the pressure was around 0.5 percent for values of $X/p$ above 36.0 and 0.1 percent for $X/p$'s of 36.0 and lower. The maximum error in field strength was about 0.1 percent. Thus, for $X/p$'s above 36.0 the total allowable error in $X$/(gas density) is 0.9 percent and the probable error about 0.3 percent. For $X/p$'s of 36.0 and lower the maximum allowable error is about 0.5 percent and the probable error less than 0.2 percent.

FREDERICK H. SANDERS

Physical Laboratory,
University of California,
Berkeley, California,
February 15, 1934.

[1] F. H. Sanders, Phys. Rev. **41**, 667 (1932); **44**, 1020 (1933).

## Rotation Spectra of $NH_3$ and $ND_3$

We have measured the pure rotation spectrum of $NH_3$, using a transmission wire grating spectrometer of large aperture. Ten lines were observed, from No. 3 at 168$\mu$ to No. 12 at 42.46$\mu$. The frequencies agree excellently with the formula calculated by Wright and Randall[1] $\nu = 19.880J - 0.00178J^3$, the average deviation being 0.12 cm$^{-1}$. The resolution attained, although inferior to that of the just-named investigators, is sufficient to give definite indication of the doublet structure in lines No. 4 to No. 6.

Preliminary measurements have been made on a sample of "heavy" ammonia, kindly supplied by Professor H. S. Taylor, the hydrogen being approximately 92 percent deuterium. The spectrum between 49 and 68$\mu$ consists of 6 sharp lines, due to $ND_3$. They have been identified as No. 20 to No. 15. Although the present accuracy is not great ($\pm 1$ cm$^{-1}$), it is sufficient to show that the lines cannot be represented by the usual formula $\nu = 2BJ - 4DJ^3$, unless $4D$ is nearly zero or even negative. We believe this is attributable to the same circumstance that causes the positions of the Raman lines $\Delta J = \pm 1$ to disagree with the usual formula:[2] namely, the existence in the energy of a small term $D_{JK}J(J+1)K^2$, due to the influence of rotations around one axis on the moment of inertia around another. The effect of such a term is to split each "line" into $J$ unresolvable components, corresponding to $0 < K < J-1$. Calculation of the relative intensity of these components shows that their center of gravity would behave much as is observed in both $NH_3$ and $ND_3$, the effect resulting in a more noticeable departure from the simple formula in the latter because the observed transitions originate on much higher energy levels. Taking this into account, we obtain for $ND_3$, $2B = 10.22 \pm 0.05$ cm$^{-1}$. This value, together with $2B = 19.88$ for $NH_3$, gives for $q_0$, the height of the ammonia pyramid, $0.34 \pm 0.03$A. The slight disagreement of this last figure with $q_0 \leqq 0.38$A, as calculated indirectly from assumed potential functions[3] is not disturbing, as the value of $\nu_4 = 770$ cm$^{-1}$, found in $ND_3$ by Silverman and Sanderson[4] is incompatible with either of the assumed functions.

It has become necessary to rebuild part of the apparatus, hence we publish these preliminary results at the present time. Needless to say, we will extend them to larger wavelengths and to the limit of our accuracy, and will discuss the theoretical implications more fully later.

R. Bowling Barnes
W. S. Benedict*
C. M. Lewis*

Palmer Physical Laboratory,
Princeton University,
Princeton, New Jersey,
February 16, 1934.

* National Research Fellows.

[1] Wright and Randall, Phys. Rev. **44**, 391 (1933).

[2] Lewis and Houston, Phys. Rev. **44**, 903 (1933).

[3] Dennison and Uhlenbeck, Phys. Rev. **41**, 313 (1932); Rosen and Morse, ibid. **42**, 210 (1932).

[4] Silverman and Sanderson, Phys. Rev. **44**, 1032 (1933); this value has also been checked in the ultraviolet by one of us (W. S. B.) and H. S. Taylor.